Evolution of cosmic magnetic fields: From the very early Universe, to recombination, to the present

Robi Banerjee[1] and Karsten Jedamzik[2]

[1]*Department of Physics and Astronomy, McMaster University, Hamilton, Ontario, Canada L8S 4M1*
[2]*Laboratoire de Physique Mathémathique et Théorique, Université de Montpellier II, 34095 Montpellier Cedex 5, France*
(Received 24 August 2004; published 6 December 2004)

A detailed numerical and analytical examination of the evolution of stochastic magnetic fields between a putative magnetogenesis era at high cosmic temperatures $T \sim 100$ MeV–100 GeV and the present epoch is presented. The analysis includes all relevant dissipation processes, such as neutrino- and photon-induced fluid viscosities as well as ambipolar and hydrogen diffusion. A simple and intuitive analytical model matching the results of the three-dimensional MHD simulations allows for the prediction of prerecombination and present day magnetic field correlation lengths and energy densities as a function of initial magnetic field energy density, helicity, and spectral index. Our conclusions are multifold. (a) Initial primordial fields with only a small amount of helicity are evolving into maximally helical fields at the present. Furthermore, the simulations show a self-similarity in the evolution of maximally helical fields implying a seemingly acausual amplification of magnetic fields on large scales is observed. (b) There exists a correlation between the strength of the magnetic field B at the peak of its spectrum and the location of the peak, given at the present epoch by $B \approx 5 \times 10^{-12}$ G(L/kpc), where L is the magnetic field correlation length determined by the initial properties of the magnetic field. (c) Concerning studies of the generation of cosmic microwave background (CMBR) anisotropies due to primordial magnetic fields of $B \sim 10^{-9}$ G on $\gtrsim 10$ Mpc scales, such fields are not only impossible to generate in early causal magnetogenesis scenarios but also seemingly ruled out by distortions of the CMBR spectrum due to magnetic field dissipation on smaller scales and the overproduction of cluster-magnetic fields. (d) The most promising detection possibility of CMBR distortions due to primordial magnetic fields may be on much smaller scales at higher multipoles $l \sim 10^6$ where the signal is predicted to be the strongest. (e) It seems possible that magnetic fields in clusters of galaxies are entirely of primordial origin, without invoking dynamo amplification. Such fields would be of (precollapse) strength 10^{-12}–10^{-11} G with correlation lengths in the kpc range and would also exist in voids of galaxies.

DOI: 10.1103/PhysRevD.70.123003 PACS numbers: 98.62.En, 98.65.Cw, 98.80.Cq

I. INTRODUCTION

Magnetic fields exist throughout the observable Universe. They exist in stars, in the interstellar medium (ISM), in galaxies, and clusters of galaxies (for a review see [1]), where in the latter two environments they are often observed with μG strength. Magnetic fields likely also reside in the intergalactic medium, though at present, their strength may be limited only by Faraday rotation measures of distant quasars [2]. The origin of galactic- and cluster-magnetic fields is still unknown. A plausible, though by far not convincingly established, possibility is the generation of magnetic seed fields and their subsequent amplification via a galactic dynamo mechanism. Seed fields may be due to a variety of processes (and with a variety of strengths), such as the Biermann battery within intergalactic shocks [3], stellar magnetic fields expelled in planetary nebulae, or during supernovae explosions, either into the intragalactic or in the presence of galactic outflows into the intergalactic medium [4], as well as due to quasar outflows of magnetized plasma [5]. Seed fields may also be of primordial origin with a multitude of proposed scenarios. These include the generation during first-order phase transitions (e.g., QCD or electroweak), around cosmic defects, or during an inflationary epoch (with, nevertheless, extremely small amplitudes), as well as before the epoch of neutrino decoupling or recombination. For a review of proposed scenarios we refer the reader to [6,7].

The philosophy in prior studies of primordial magnetogenesis is often (but not always) as follows. After establishing a battery mechanism (e.g., separation of charges and production of currents) and a ''prescription'' or estimate for the final, nonlinearly evolved magnetic field strength (e.g., equipartition with turbulent flows), subsequent evolution is approximated by simply assuming frozen-in magnetic field lines into the plasma. Though this may be appropriate on the very largest scales, it should be clear that this may not be the case on the *fundamental* coherence scale of the field. Here, coupling of the magnetic fields to the gas induces nonlinear cascades of energy in Fourier space. The characteristics of initially created magnetic field are thus vastly modified during cosmic evolution between the epoch of magnetogenesis and the present. The final step in such studies is then often to determine field strengths on some prescribed scale (e.g., 10 Mpc) typically falling in the range $10^{-30} \lesssim B \lesssim 10^{-20}$ G, inferring that this may be sufficient to seed

an efficient dynamo for the production of galactic- and cluster-magnetic fields. This is observed in negligence of the fact that much stronger fields on smaller scales result not only from a variety of astrophysical seeds, but from these very same primordial scenarios.

Considering the likelihood of a magnetized early Universe (i.e., due to the large number of charged particles and the multitude possible of *out-of-equilibrium* processes) it should be instructive to develop a somewhat complete picture of magnetic field evolution in the early Universe, subsequent to the epoch of magnetogenesis. This should be accomplished *irrespective* of such fields providing the seeds for galactic fields or not. For example, it may be that at some later time relatively weak field strengths in galactic voids are measurable via the propagation of the highest energy-cosmic rays [8,9], or via accurate measurements of γ-ray bursts [10]. The interpretation of such putative measurements, which could hint to fields of primordial origin, is then possible only if one understands the evolution of these fields between magnetogenesis and the present.

One step in this direction has been performed by Dimopoulos and Davis [11] as well as Son [12] who exactly considered such nonlinear processing of magnetic fields due to magnetohydrodynamic cascades in the early Universe. Another step has been provided by Jedamzik *et al.* [13] (hereafter, JKO98) and shortly after by Subramanian and Barrow [14] who considered fluid-viscosity (due to neutrinos and photons) induced damping of magnetic fields. The study by Son, though describing appropriately the gross nonlinear features of MHD evolution, does not properly deal with the effect of fluid viscosity [15], with the net effect of estimates of present day coherence lengths being orders of magnitude smaller than those we find. Moreover, this study, as most others, does not provide explicit expressions for the final magnetic field energy. The study in Ref. [11], on the other hand, though examining the effect of photon drag before recombination, employs a somewhat particular model of magnetic field coherence length growth which is not supported by results of numerical simulations. The study by JKO98 is strictly speaking applicable only in the linear regime (i.e., under the assumption of a homogeneous background magnetic field), whereas Subramanian and Barrow also considered a limited class of nonlinear configurations. Results of both studies on the magnetic field coherence length at recombination are identical to those found in the nonlinear analysis attempted here. Nevertheless, at intermediate stages of evolution (i.e., well before recombination) the predicted magnetic coherence length in these studies deviates from that found here. Moreover, none of these works discusses the effects of ambipolar diffusion after the epoch of recombination, neither verifies claims by complete three-dimensional numerical simulations.

Two-dimensional (e.g., [16]) and three-dimensional (e.g., [17]) numerical simulations of magnetohydrodynamics in the early Universe were performed in the context of maximal helical fields. Similarly, effective three-dimensional cascade models [12] have also been employed. Helicity of primordial magnetic fields could play an important role, as noted by a number of authors [12,18–22], as it may significantly speed up the growth of magnetic field coherence length, thereby leading to potentially large magnetic fields strengths on comparatively large scales ($\sim$ 1–10 kpc depending on the amount of initial helicity). It has also been argued that a net primordial magnetic helicity may be potentially linked to the cosmic baryon-to-entropy ratio (e.g., [18,21]). Adopted models of field evolution are either appropriate to turbulent evolution [20], or to viscous evolution (i.e., assuming a drag force due to photons [22]). Before passing, we also note studies of the effects of magnetic fields on the cosmic microwave background radiation (CMBR), as, for example, the generation of temperature anisotropies below [23,24] or above [25] the Silk damping scale, as well as the distortions of the CMBR Planck spectrum by magnetic field dissipation [26]. These studies have also to include certain evolutionary features of magnetic fields, but due to the largeness of the Silk scale ($\sim$ 10 Mpc comoving) backreaction of the peculiar flows generated by magnetic fields on the magnetic fields themselves. This is in contrast to the importance of backreaction on the typically much smaller magnetic field coherence scale (such as for the analysis in [26]).

In this paper we attempt to provide a unified picture for the gross features of magnetic field evolution in the early Universe. As a function of the initial conditions for the magnetic fields generated during a putative magnetogenesis era, we predict the magnetic field coherence length and magnetic-energy density for all subsequent epochs for fields of arbitrary strength and helicity. Our treatment incorporates all the relevant dissipative processes, in particular, due to photon and neutrino diffusion as well as free streaming, and due to ambipolar and hydrogen diffusion.

The outline of the paper is as follows. While many of the preliminaries to the discussion, such as the equations, treatment of Hubble expansion, and magnitudes of dissipative terms, are deferred to the appendixes, Sec. II immediately commences with a discussion of turbulent MHD cascades and the presentation of results of three-dimensional numerical simulations. In Sec. III magnetic field evolution in the viscous regime before recombination (which is a regime particular to the early Universe) is discussed and numerically simulated, whereas Sec. IV discusses the effects of ambipolar diffusion after recombination. The general picture and detailed analytical results for cosmic magnetic field evolution are developed in Sec. V, whereas Sec. VI provides a discussion of the high-

lights of our findings. In the Appendixes A and B we compile the MHD equations appropriate for the study of magnetohydrodynamics in the expanding Universe, whereas Appendix C compiles the various dissipation terms in the early Universe. Details on the generation of helical fields are given in Appendix D and details on the numerical simulations in Appendix E.

II. TURBULENT MAGNETOHYDRODYNAMICS

In this section we discuss general features of the evolution of magnetized fluids in the turbulent regime (Reynolds number $R_e \gg 1$ as applicable well before neutrino coupling and recombination), such as the decay of energy density as well as the growth of magnetic field coherence length. The exceedingly large Prandtl numbers (cf. Appendix C) in the early Universe allow one to neglect dissipative effects due to finite conductivity. Further, the generation of primordial magnetic fields in magnetogenesis scenarios is generally believed to occur during well-defined periods (e.g., QCD transition). Subsequent evolution of these magnetic fields is therefore described as a *free decay* without any further input of kinetic or magnetic energy, i.e., as freely decaying MHD. Because of the largeness of the speed of sound in a relativistic plasma $v_s = 1/\sqrt{3}$, the assumption of incompressibility of the fluid is appropriate during most epochs, as well as for a large range of initial magnetic field configurations and energy densities. An exception to the incompressibility may occur for initial conditions which result in magnetic fields of strength $B \gtrsim 6 \times 10^{-11}$ G (comoving to the present epoch, cf. Sec. V) and only after the decoupling of photons from the flow.

To verify theoretical expectations we have performed numerical simulations of incompressible, freely decaying, ideal, but viscous MHD. These simulations are performed with the help of a modified version of the code ZEUS-3D [27–29] in a nonexpanding (Minkowski) background. Modifications lie in the inclusion of fluid viscosities, e.g., a drag coefficient α as given in Eqs. (3), (C8), and (C9). From the discussion in Appendix B it should be clear that for most purposes results of numerical simulations with existing (or slightly extended) codes with Minkowski metric may be reinterpreted into results of MHD in an expanding universe with Friedmann-Robertson-Walker (FRW) metric, when rescaled variables as given in the Appendix are considered. For details of the numerical simulations the reader is referred to Appendix E.

Incompressible MHD is described by the following equations (for the equations of compressible MHD the reader is referred to Appendixes A and B):

$$\frac{\partial \mathbf{v}}{\partial t} + (\mathbf{v}\cdot\nabla)\mathbf{v} - (\mathbf{v}_\mathrm{A}\cdot\nabla)\mathbf{v}_\mathrm{A} = \mathbf{f}, \tag{1}$$

$$\frac{\partial \mathbf{v}_\mathrm{A}}{\partial t} + (\mathbf{v}\cdot\nabla)\mathbf{v}_\mathrm{A} - (\mathbf{v}_\mathrm{A}\cdot\nabla)\mathbf{v} = \nu\nabla^2\mathbf{v}_\mathrm{A}, \tag{2}$$

where we have defined a *local* Alfvén velocity $\mathbf{v}_\mathrm{A}(x) = \mathbf{B}(x)/\sqrt{4\pi(\varrho + p)}$, and where $\mathbf{v}$, $\mathbf{B}$, ϱ, and p are the velocity, magnetic field, mass-energy density, and pressure, respectively. Here fluid dissipative terms in the Euler equation are given by

$$\mathbf{f} = \begin{cases} \eta\nabla^2\mathbf{v} & l_\mathrm{mfp} \ll l, \\ -\alpha\mathbf{v} & l_\mathrm{mfp} \gg l, \end{cases} \tag{3}$$

where there exists a distinction between dissipation due to diffusing particles, with mean free path smaller than the characteristic scale $l_\mathrm{mfp} \ll L$, or dissipation due to a free-streaming (i.e., $l_\mathrm{mfp} \gg L$) *background* component exerting drag on the fluid by occasional scatterings with fluid particles. Both regimes are of importance in the early Universe as already noted in JKO98. Note that in the computation of $\mathbf{v}_\mathrm{A}$ only those particles with $l_\mathrm{mfp} \ll L$ contribute to ϱ and p. An important characteristics of the fluid flow is given by its local kinetic Reynolds number

$$R_e(l) = \frac{v^2/l}{|\mathbf{f}|} = \begin{cases} \frac{vl}{\eta} & l_\mathrm{mfp} \ll l \\ \frac{v}{\alpha l} & l_\mathrm{mfp} \gg l, \end{cases} \tag{4}$$

with l some length scale. The Reynolds number is a measure of the relative importance of fluid advective terms and dissipative terms in the Euler equation, given by the ratio of a typical dissipative time scale $\tau_d = (l^2/\eta, 1/\alpha)$ to the *eddy-turnover time scale* $\tau_\mathrm{eddy} = l/v$. For most magnetic field configurations it is possible to define an *integral scale*, L, i.e., the scale which contains most of the magnetic and fluid kinetic energy. We will frequently refer to this scale as the *coherence scale* or *coherence length* of the magnetic field. In the case of *turbulent* flow, with $R_e(L) \gg 1$ on this scale, the decay rate of the total energy is independent of dissipative terms and depends only on the flow properties on the integral scale. This is in contrast to the decay of magnetic and fluid energy in the *viscous* regime, $R_e(L) \ll 1$, where the total decay rate depends on the magnitude of viscosities. In the following, the dynamic evolution of magnetic fields in the former (turbulent) regime will be studied.

A. Nonhelical fields

Consider Eqs. (1) and (2) with a stochastic, statistically isotropic, magnetic field and, for the purpose of illustration, with initially zero fluid velocities. For the moment we will also assume that the magnetic field does not possess any net helicity. In the limit of large Reynolds numbers on the coherence scale, the dissipative term may be neglected on this scale. Magnetic stresses [the third term on the left-hand side (LHS) of Eq. (1)] will establish fluid motions of the order $v \approx v_\mathrm{A}$ within an Alfvén

crossing time $\tau_A \approx l/v_A$, at which point backreaction of the fluid flow on the magnetic fields will prevent further conversion of magnetic field energy into kinetic energy. The resultant fully turbulent state is characterized by close-to-perfect equipartition (in the absence of net helicity)

$$\langle \mathbf{v}^2 \rangle \approx \langle \mathbf{v}_A^2 \rangle, \tag{5}$$

between magnetic and kinetic energy. This may be seen in Fig. 1, which shows the decay of magnetic and kinetic energies in freely decaying turbulent MHD.

Nonlinear MHD processes quickly establish turbulence on scales below the integral scale (cf. Fig. 2). Working with Fourier transforms (assuming statistical isotropy and homogeneity) and defining the total magnetic- and kinetic-energy densities

$$E \approx \int d\ln k k^3 (\langle |v_k|^2 \rangle + \langle |v_{A,k}|^2 \rangle) \equiv \int d\ln k E_l, \tag{6}$$

one finds that a typical root-mean-square velocity perturbation on scale $l = 2\pi/k$ is $v_l \approx \sqrt{k^3 \langle |v_k|^2 \rangle} \approx \sqrt{E_l}$. Note that in the above and for the remainder of this section we set $(\varrho + p)/2 = 1$ [cf. Eq. (C1)], as frequently done in studies of incompressible MHD, such that energy density has the dimension of velocity square. By inspection of the Fourier transformed Eqs. (C3) and (C4) it may be seen that dissipation of energy is dominated by flows on the smallest scales (largest k), given that energy spectra E_l fall not too steeply with growing k. Dissipation of energy into heat thus occurs at some much smaller-scale $l_{\rm diss} \ll L$ [where $R_e(l) \approx 1$]. The transport of the fluid energy from the integral scale L to the dissipation scale $l_{\rm diss}$ occurs via a cascading of energy from large scales to small scales, referred to as *direct cascade.*

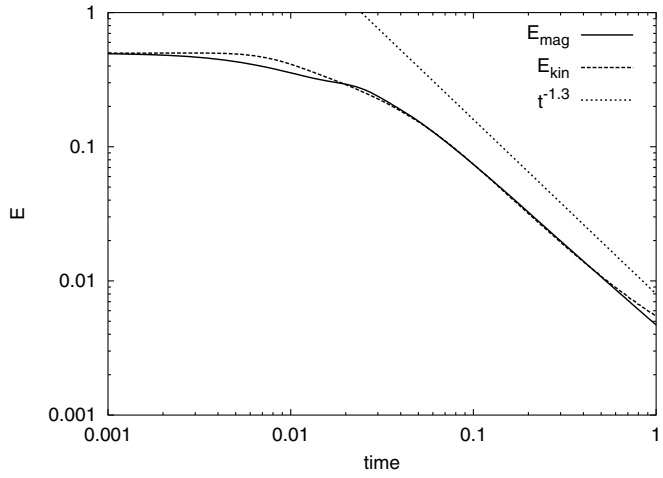

FIG. 1. Comparison of the time evolution of the magnetic (solid line) and the kinetic (dashed line) energy in the turbulent regime ($R_e \gg 1$) for a magnetic field without initial helicity. For comparison, also the theoretical damping law, $E \propto t^{-1.3}$, is shown (dotted line). Here, the simulation was performed on a mesh with 128^3 grid points and the magnetic field is excited up to $k_c \approx 16$ with a spectral index $n \approx 4$ [cf. Eqs. (8) and (9) and Appendix E].

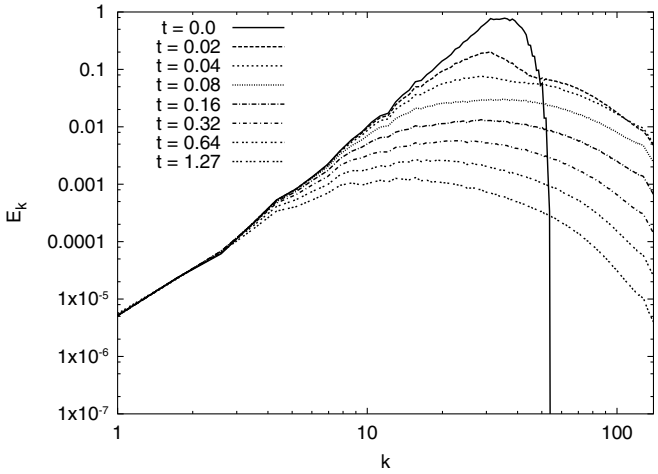

FIG. 2. Evolution of magnetic-energy spectra in the turbulent regime for a magnetic field with no initial helicity. Here, the spectral index of the initial energy spectra is $n \approx 4$.

Ever since the work of Kolmogorov it is known that this cascading of energy occurs as a quasilocal process in k space, with flow eddies on a particular scale l breaking up into eddies of somewhat smaller scale $\sim l/2$. This continuous flow of energy through k space,

$$\frac{dE_l}{dt} \approx \frac{E_l}{\tau_l} \approx \text{const}(k), \tag{7}$$

results in a quasistationary energy spectrum on scales $l \lesssim L$, with energy flow rates approximately independent of a wave vector. We remind the reader that throughout L denotes the integral scale. Typical energy dissipation times τ_L are given by an eddy-turnover time at the integral scale $\tau_L \sim \tau_{\rm eddy} \approx L/v_L \sim L/(\sqrt{E_L})$.

Although the "Kolmogorov hypothesis," Eq. (7), is well established in turbulence studies in both the pure hydrodynamic case as well as in MHD turbulence, the resulting decay spectra (E_l for $l < L$) in MHD turbulence is not. Early attempts by Iroshnikov [30] and Kraichnan [31] (IK) to explain the cascading spectrum of MHD turbulence by assuming isotropy in k space were shown to be incorrect first by Goldreich and Sridhar [32]. Goldreich and Sridhar established that MHD turbulence is intrinsically anisotropic with eddies elongated in the direction of the background (integral scale) magnetic field (i.e., $k_\parallel \approx k_\perp^{2/3} L^{-1/3}$ where $k_\parallel$ and $k_\perp$ are wave vectors parallel and perpendicular to the background magnetic field $v_{A,L}$) and energy cascading more rapidly in $k_\perp$ space orthogonal to the magnetic field. Though the predicted anisotropy has been observed in numerical simulations, the predicted modification of the MHD spectra, in particular, the existence of "one-dimensional"

Kolmogorov-type spectra $\tilde{E}_k = E_k/k \propto k_\perp^{-5/3}$ has not been [33]. Rather, these spectra seem to have a shallower slope with a spectral index of $\approx -3/2$. In contrast, Müller and Biskamp [34] find "three-dimensional" energy spectra consistent with a Kolmogorov spectra. Inspection of Fig. 2, which shows such three-dimensional spectra in our 256^3 numerical simulations of freely decaying MHD, illustrates how difficult it is to distinguish between exponents $-5/3$ and $-3/2$. This is due to the *inertial range* between the dissipation scale (here given by a few times the Nyquist frequency due to numerical dissipation) and the integral scale being rather small. Moreover, both scales do not seem to be well defined, resulting in a small-scale spectrum more consistent with an exponential than a power law. This is also not significantly changed when one proceeds to 512^3 simulations, such that a numerical confirmation of one, or the other, spectrum may be premature.

In this work we do not account for the possible effect of intermittency, i.e., the non random distribution of eddies in space, on the dynamics of MHD turbulence (see e.g. [35]). The appearance of intermittency can in principle modify the turbulent spectra but it has been shown that it does not affect the inertial-range dynamics (see [33] and references therein).

Evolution of global properties of the magnetic field in freely decaying MHD, such as total energy density and coherence length, depend on the magnetic field spectra on scales above the integral scale, $l > L$, and are related to initial conditions. Consider an initial magnetic field with blue spectrum,

$$E_k \approx E_0\left(\frac{k}{k_0}\right)^n = E_0\left(\frac{l}{L_0}\right)^{-n} \quad \text{for } l > L_0. \tag{8}$$

The scale-dependent relaxation time, $\tau_l \approx l/v_{\mathrm{A},l} \approx l/\sqrt{E_l}$ (with $v_{\mathrm{A},l} = \sqrt{k^3\langle|\boldsymbol{v}_{\mathrm{A},k}|^2\rangle}$) increases with scale as $\tau_l \propto l^{1+n/2}$. Transfer of magnetic energy to kinetic energy and a fully developed turbulent state may only occur for times $t \gtrsim \tau_l$. When such a state is reached the energy on this scale decays through the cascading of large-scale eddies to smaller-scale eddies down to the dissipation scale. Since the relaxation time for the "next" larger scale l is longer, this larger scale now starts to dominate the energy density, i.e., becoming the integral or coherence scale. This is sometimes referred to as *selective decay* of modes in k space. The remaining energy density is then the initial energy density of modes between the very largest scales and this next larger scale. Given these arguments and the initial spectrum of Eq. (8) one then may derive for the time evolution of energy and coherence length of the magnetic field

$$\begin{aligned} &E \approx E_0\left(\frac{t}{\tau_0}\right)^{-2n/(2+n)} \quad L \approx L_0\left(\frac{t}{\tau_0}\right)^{2/(2+n)} \quad \text{no helicity,} \\ &R_e \gg 1, \end{aligned} \tag{9}$$

for $t \gtrsim \tau_0$, where τ_0 is the relaxation time on the scale L_0, i.e., $\tau_0 \approx L_0/\sqrt{E_0} \approx L_0/v^{\mathrm{A}}_{L,0}$, and where indices 0 denote quantities at the initial time. For instance, for a spectral index of $n = 3$ (which corresponds to the large-scale magnetic field due to a large number of randomly oriented and homogeneously distributed magnetic dipoles [36]) the energy density follows $E \propto t^{-6/5}$ which is Saffman's law known from fluid dynamics [37,38].

An increase of the magnetic field coherence scale with time due to selective decay may be observed in Fig. 2, whereas the decay of magnetic-energy density for a variety of initial magnetic field spectra is shown in Fig. 3. It can be seen that initial spectra with larger n indeed lead to a more rapid decrease of energy with time as predicted by Eq. (9). Nevertheless, comparison of the theoretically expected decay exponents [cf. Eq. (9)] to the numerically found exponents (cf. Fig. 3) indicate slight differences. Generally, our numerical simulations result in a slower energy decay than predicted by Eq. (9). For example, the theoretically predicted damping exponent, i.e., $E(t) \propto t^{-\gamma}$, for a $n = 3$ initial energy spectrum is $\gamma = 1.2$ whereas the best fit of our numerical simulations gives $\gamma \approx 1.05$. It is not easy to find a physical explanation for this, as it would entail an additional *with time increasing* slowdown of relaxation at large scales $l \gtrsim L$ and/or a slowdown of energy dissipation of already turbulent modes at small scales $l \lesssim L$. In either case, to explain such a phenomenon a quantity with physical dimension of

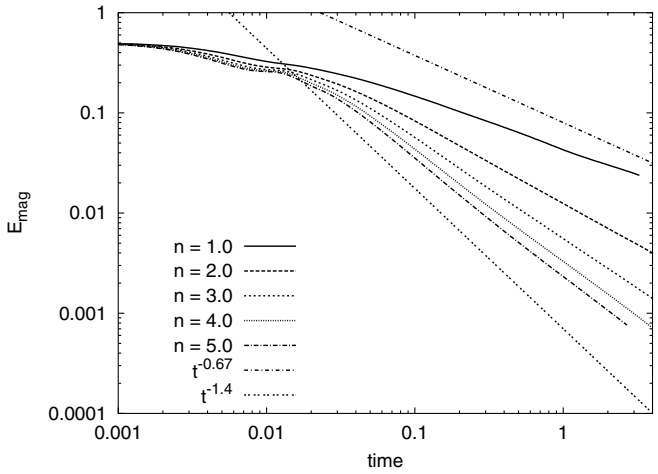

FIG. 3. The evolution of the magnetic energy in the turbulent regime for different initial energy spectra n, where $E_k = k^3|b_k|^2 \propto k^n$ with a cutoff $k_c \approx 32$. Here, the initial magnetic field is nonhelical. In this case, the damping law depends on the spectral index [cf. Eq. (9)]. For comparison, the theoretical predicted damping laws for $n = 1$ ($E \propto t^{-0.67}$) and for $n = 5$ ($E \propto t^{-1.4}$) are also shown.

length or velocity, which has not yet entered the analysis, should exist. Given that the assumed initial magnetic field distribution is statistically self-similar on different scales, and that helicity is negligible, this quantity may only be the dissipation length and/or length of the simulation box. Whereas the latter is a complete numerical artifact, the former is so widely separated from the integral scale during most periods of the high Reynolds number flow in the early Universe that we expect it not to influence the dynamics on the integral scale. We have noted that spectra at late times show a peak region ΔL quite spread and are likely only marginally resolved by the simulations. In any case, larger numerical simulations are required to address this effect seen also by others (e.g., [17,39]).

B. Helical fields

We have so far studied the evolution of a statistically isotropic and homogeneous magnetic field in the absence of net helicity (see Appendixes C and D for the definition and dissipation of magnetic helicity). Given that magnetic helicity should be an ideal invariant in the early Universe (where the conductivity is almost perfect), and that magnetic fields with even small initial net helicity ultimately reach maximal helicity density

$$\mathcal{H} \lesssim \mathcal{H}_{\max} \approx \langle B^2 L \rangle \approx (8\pi) EL, \tag{10}$$

it should be of importance to also study the maximally helical case. Note that, a maximally helical state is reached during the course of MHD turbulent evolution due to a slower decay of the helical component of fields as compared to the nonhelical one [cf. Eqs. (9) and (12)]. When maximal helicity is reached magnetic field evolution is significantly altered with respect to the case of zero, or submaximal helicity. Figure 4 shows the results of 256^3 simulations of the evolution of the ratio between kinetic- and magnetic-energy density Γ assuming initial conditions of a maximally helical field and negligible velocity perturbations. After a relaxation time of the order of the Alfvén crossing time $L/v_{A,L}$ over the integral scale a quasisteady state with constant $\Gamma \approx 0.2$ develops. Note that in contrast to the turbulent, nonhelical case, full equipartition is not reached. The associated spectrum of Γ is shown in Fig. 5 showing that at the integral scale kinetic-energy density is always smaller than magnetic-energy density. Though not apparent from the figure, an integral scale (i.e., the scale of maximum energy density) defined for kinetic-energy density only $L^{\rm kin}$ trails the integral scale for total energy density with time, i.e., $L^{\rm kin}/L < 1$ with a ratio approximately constant in time. Magnetic field spectra for this simulation are shown in Fig. 6. It is seen that *inertial-range* magnetic spectra at $l \lesssim L$ are well described by power laws over a limited range in k space. For this exponent ($n = 4$) we find $E_k \propto k^{\beta}$, $\beta \approx -1.7$, significantly steeper than either Komogorov or IK.

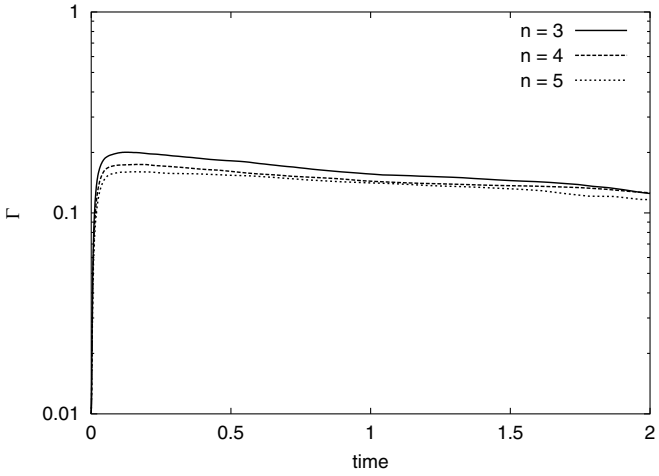

FIG. 4. Time evolution of $\Gamma = E_{\rm kin}/E_{\rm mag}$ for maximal helical magnetic fields with different spectral indices n in the turbulent regime. The initial kinetic energy is set to $10^{-4} E_{\rm mag}$. The ratio Γ is nearly constant in time, although, equipartition of kinetic and magnetic energy is not established for helical magnetic fields.

Figure 6 also illustrates the intriguing property of self-similarity of spectra at different times. This phenomenon of self-similarity has also been observed by [17]. Magnetic field amplification on very large scales occurs even at times much shorter than the typical relaxation time for magnetic fields (i.e., Alfvén crossing time) on these scales, indicating the topological constraint (by helicity) imposed on the field evolution. Note that if magnetic fields on large scales would not be enhanced,

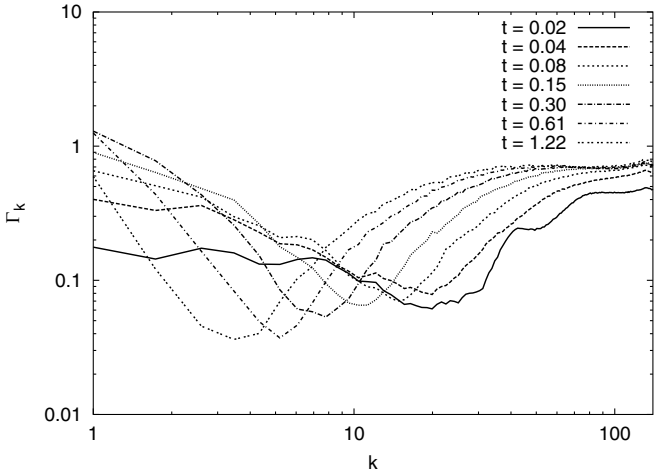

FIG. 5. The evolution of the ratio of the kinetic- and magnetic-energy spectrum $\Gamma_k = E_k^{\rm kin}/E_k^{\rm mag}$ for a maximal helical magnetic field in the turbulent regime. In this case equipartition ($\Gamma_k \approx 1$) is established only on very small scales. At the integral scale the kinetic energy is always much smaller than the magnetic energy.

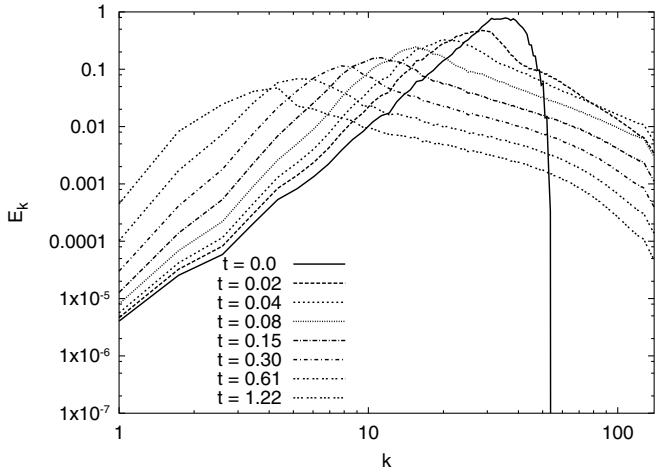

FIG. 6. Evolution of magnetic-energy spectra in the turbulent regime for magnetic fields with initially maximal helicity. The spectral index of the energy spectra is $n \approx 4$.

magnetic coherence length could not grow with time, as generally the initially existing energy density on large scales would not suffice to keep $\mathcal{H}$ constant. Having performed simulations of maximally helical fields with different initial spectral indices n we have noted that though the amplitude of a large-scale magnetic field grows with time, the spectral index of the magnetic field configuration on large scales seems to be approximately preserved.

There seems to be a misconception in the literature (see, e.g., [20,21]) that maximally helical fields do not dissipate energy via excitation of fluid flows and the subsequent dissipation of these flows due to fluid viscosities. It is argued, that maximally helical fields with a fairly peaked spectrum are essentially force free [i.e., $\mathbf{v}_\mathrm{A} \times (\nabla \times \mathbf{v}_\mathrm{A}) \approx 0$] and may thus not excite fluid flows. Note that if this indeed would be the case, Eq. (2) would imply trivial magnetic field evolution $\mathbf{B} = \text{const}$ for initially zero velocity fluctuations and resistivity. Though the magnetic stresses in the Euler equation are indeed found smaller for a maximally helical field as compared to a nonhelical field of similar strength, an increase of magnetic coherence length and the continuous excitation of subequipartition fluid flows are observed in our simulations. It may be that such fluid excitations are due to force-free magnetic field configurations being unstable equilibria. In any case, in the limit of large Prandtl number, dissipation of these flows will provide the main dissipation of magnetic field energy.

The decay rate of total magnetic energy in freely decaying MHD turbulence of maximally helical fields may be well approximated by the decay rate of energy on the integral scale

$$\frac{dE}{dt} \approx \frac{E}{\tau_L} \approx \frac{E^{3/2}}{L}\Gamma \sim \frac{E^{5/2}}{\mathcal{H}}\Gamma, \tag{11}$$

where $\tau_L \approx L/v_{\mathrm{A},L}$, and Eq. (10) for a maximally helical field has been employed in the second step. Since $\mathcal{H}$ and Γ (see Appendix C and Fig. 4) are constant it is straightforward to derive the power-law exponents for the decay of energy and growth of coherence length with time

$$E \approx E_0\left(\frac{t}{\tau_0}\right)^{-2/3} \approx L_0\left(\frac{t}{\tau_0}\right)^{2/3} \text{ maximal helicity,} \quad R_e \gg 1, \tag{12}$$

for $t \gtrsim \tau_0 \approx L_0/\sqrt{E_0} \approx L_0/v^\mathrm{A}_{L,0}$, yielding a predicted decay which is independent of the spectral index of the large-scale magnetic field. The correctness of Eq. (12) has been recently questioned by Biskamp and Müller [40]. These authors advocate a decay of kinetic energy with time as $\Gamma \propto E/\mathcal{H}$, yielding a modified Eq. (12) $dE/dt \sim E^3/\mathcal{H}^{3/2}$, and energy decay $E \propto t^{-1/2}$. We note here that a decay of Γ was not found in our simulations. Moreover, a relationship $\Gamma \propto E/\mathcal{H}$ is dimensionally incorrect, and must be modified by an as yet unknown quantity of dimension length. Because of the absence of a physically well-motivated choice for this quantity (other than l_diss or L_box), we suspect their results to be an artifact of limited resolution. In particular, Biskamp and Müller [40] observe a decay in Γ only at late times, when the coherence scale has already moved dangerously close to L_box. Note, that larger kinetic (numerical) viscosities result in larger magnetic dissipation times (cf. Sec. III). Therefore, the rather moderate Reynolds numbers [$\mathcal{O}(10^3)$] achieved in numerical simulations could be responsible for the slower decay rates found in these simulations.

Figure 7 shows the total magnetic energy as a function of time for a variety of maximally helical magnetic fields

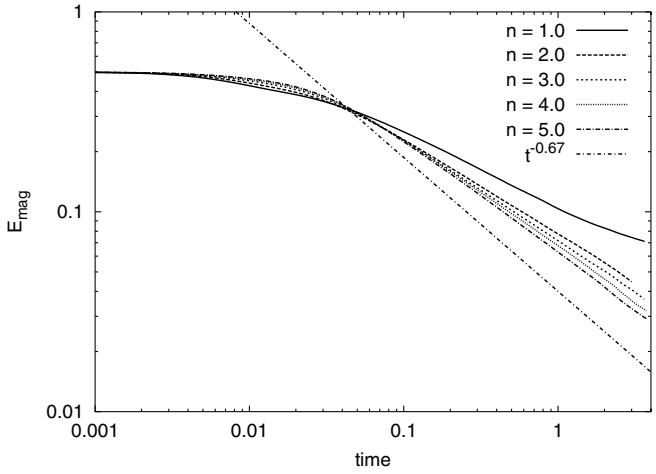

FIG. 7. The evolution of the magnetic energy in the turbulent regime for different initial energy spectra n, where $E_k = k^3|b_k|^2 \propto k^n$. Here, the initial magnetic field is maximal helical. For comparison, also the theoretical damping law, $E \propto t^{-0.67}$, is shown. In contrast to the nonhelical case, the damping law for a helical magnetic field is nearly independent of the spectral index n for $n < 1$.

of different initial spectral index. With the exception of the rather red spectrum $n = 1$, for which the Fourier transform of helicity is not peaked in k space, the decay of energy seems to be indeed approximately independent of spectral index. Residual dependencies on n may possibly be associated with the nonconservation of helicity as shown in Fig. 8. This dissipation of helicity in our simulations is due to numerical dissipation at the Nyquist frequency. Similar to the case of nonhelical fields, the decay slopes observed in the simulations are somewhat shallower than those predicted by Eq. (12). For example, for $n = 5$ we find a damping exponent of $\gamma \approx 0.5$ (coincidentally agreeing with [40]). Arguments very similar to those presented at the end of the previous paragraph, in particular, the absence of a quantity of dimension length or velocity beyond those employed in Eq. (12), make us believe this deviation to be unphysical.

To complete this section we would like to mention that the magnetic helicity might evolve differently if the decay spectra of the magnetic field is not declining towards smaller scales. For instance such a situation can be achieved if the turbulence is not freely decaying but driven by turbulent energy input at a certain scale. Studies of multiscale turbulence show that helicity peaks appear at the integral scale as well as at the driving scale [41]. However, scenarios like this are hard to envision in the mostly quiescent early Universe, due to the absence of turbulent energy injection, except during brief periods (i.e., cosmic first-order phase transitions). MHD turbulence in the early Universe should therefore be adequately described as freely decaying.

III. VISCOUS MAGNETOHYDRODYNAMICS

Magnetic field dissipation in high Prandtl number fluids may also occur in the viscous regime, where kinetic Reynolds numbers are much smaller than unity. Of particular importance to MHD evolution in the early Universe is the case of photons or neutrinos free streaming over the scales of interest, $l_{\rm mfp} \gg l$, resulting in a drag force in Eq. (1) with drag coefficient α. Such "dragged" MHD is rare in other astrophysical environments. One exception might by the drag exerted by neutral atoms on the magnetized ISM (see [42] for analytic results of the cascading spectra). To our knowledge numerical simulations of this regime have so far not been performed.

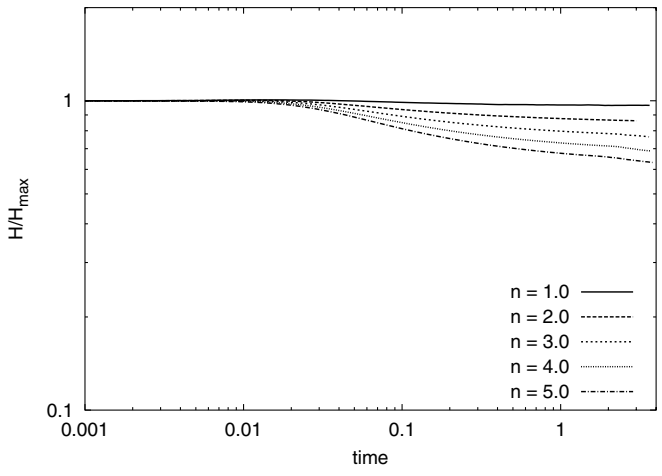

FIG. 8. Evolution of helicity as a function of time for different spectral indices n. Note that in the case of no numerical diffusion $\mathcal{H}(t)/\mathcal{H}_{\rm max} = 1$ should be achieved.

Consider again the Euler equation (1). Whereas in the turbulent case there is a balance of the terms on the LHS, which are all of similar magnitude, in the dragged case there is a balance between the last term on the right-hand side (RHS) and the dissipative term f, with all other terms negligible. In the terminal velocity regime one finds thus [using Eq. (3)]

$$\mathbf{v} \approx \frac{1}{\alpha}(\mathbf{v}_{\rm A} \cdot \nabla)\mathbf{v}_{\rm A} \tag{13}$$

such that $v_l \approx v_{{\rm A},L}(\tau_{\rm drag}/\tau_{{\rm A},l}) \ll v_{{\rm A},l}$ for $\tau_{\rm drag} \equiv \alpha^{-1} \ll \tau_{{\rm A},l}$. This yields a kinetic Reynolds number of

$$R_e \approx \left(\frac{v_{{\rm A},l}}{\alpha l}\right)^2 \ll 1. \tag{14}$$

Though one would naively expect that at small Reynolds number the total energy gets immediately dissipated due to viscous terms, this is not the case (JKO98). For large Prandtl number the energy may only be dissipated via the excitation of fluid motions. Nevertheless, due to the strong drag, such excitation is slow and inefficient, and a system with $\Gamma \ll 1$, i.e., well below equipartition between magnetic- and kinetic-energy results. Since the dissipation rate is proportional to the velocity fluctuations v the net effect of strong fluid viscosities is a delayed dissipation and quasi-frozen-in magnetic fields. Note that in the case of viscous MHD, flows are effectively dissipated on the integral scale, and cascading of energy in k space is not required. One finds for the energy dissipation rate

$$\frac{dE}{dt} \approx \frac{E}{\tau_L} \sim \frac{E^2}{L^2\alpha}, \quad \text{with } \tau_L \approx L/v_L \sim \frac{L^2\alpha}{E}, \tag{15}$$

and where τ_L is a formal *eddy* turnover time scale identical to the *overdamped* time scale for the evolution of overdamped Alfvén and slow-magnetosonic modes as found in JKO98.

A. Nonhelical fields

With a blue spectrum ($n > 0$) for the magnetic fields on large scales as given in Eq. (8), and with very similar reasoning as in the turbulent case, one may compute the asymptotic power law for decay of energy density and growth of magnetic field coherence length as

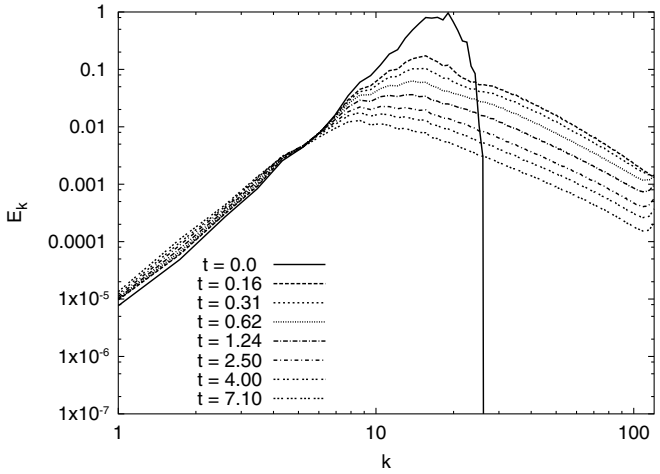

FIG. 9. The evolution of the magnetic-energy spectra in the viscous free-streaming regime ($R_e \ll 1$) for a magnetic field without initial helicity. The simulations were performed on a mesh with 256^3 grid points, and the cutoff is $k_c \approx 16$.

$$E \approx E_0\left(\frac{t}{\tau_0^{\rm visc}}\right)^{-n/(n+2)} L \approx L_0\left(\frac{t}{\tau_0^{\rm visc}}\right)^{1/(n+2)} \text{ no helicity,} \quad R_e \ll 1, \tag{16}$$

for $t \gtrsim \tau_0^{\rm visc}$ and where $\tau_0^{\rm visc} \approx \tau_{L,0}^{\rm A}(\tau_{L,0}^{\rm A}/\tau_{\rm drag}) \approx L_0^2\alpha/E_0$. Here, in contrast to the condition in the early Universe, a constant (in time) drag coefficient α has been assumed. Note that Eq. (16) indeed predicts slower magnetic field energy decay than its counterpart Eq. (9) in the turbulent case, in particular, a longer relaxation time $\tau_0^{\rm visc} \gg \tau_0$ and smaller decay slope $\gamma_{\rm visc} = \gamma_{\rm turb}/2$ for the energy density. In Figs. 9 and 10 results of our numerical simulations of viscous nonhelical MHD in the free-streaming regime are shown. For times longer than the relaxation time on the integral scale, small-scale power spectra are well described by power laws $E_k \propto k^\beta$ of exponent $\beta \approx -2.0$. This power law is approximately consistent with a Reynolds number $R_{e,l} \sim \text{const}(l)$ independent of scale l. Figure 11 illustrates that Eq. (16) is a good approximation to the numerical simulations, though numerically simulated fields tend to decay somewhat slower than predicted, as observed in the sections before.

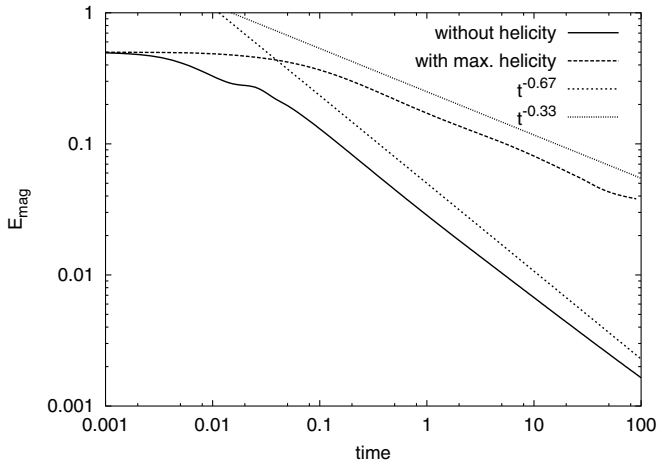

FIG. 10. Evolution of the magnetic energy without (solid line) and with maximal (dashed line) initial helicity in the viscous free-streaming regime ($R_e \ll 1$). The simulations were performed on a mesh with 128^3 grid points, the cutoff is $k_c \approx 16$, and the spectral index $n \approx 4$. For comparison, also the theoretical expected damping laws are shown, i.e., $E_{\rm mag} \propto t^{-0.67}$ (without helicity) and $E_{\rm mag} \propto t^{-0.33}$ (with maximal helicity).

B. Helical fields

In the case of maximally helical fields one may use the constancy of helicity density in Eq. (10) to find

$$\frac{dE}{dt} \sim \frac{E^4}{\mathcal{H}^2\alpha}, \tag{17}$$

yielding

$$E \approx E_0\left(\frac{t}{\tau_0^{\rm visc}}\right)^{-1/3} L \approx L_0\left(\frac{t}{\tau_0^{\rm visc}}\right)^{1/3} \text{ maximal helicity,} \quad R_e \ll 1, \tag{18}$$

where $\tau_0^{\rm visc}$ is as before. Results of our numerical simulations for this case may be found in Figs. 10 and 11. As in the nonhelical case these are consistent with a small-scale power-law spectrum $E_k \propto k^\beta$ with $\beta \approx -2.0$. Note that, in contrast to before, agreement of Eq. (18) and the simulation seems excellent.

IV. MHD WITH AMBIPOLAR DIFFUSION

After recombination the Universe is only weakly ionized (i.e., $X_e \ll 1$). Neutral particles, i.e., hydrogen

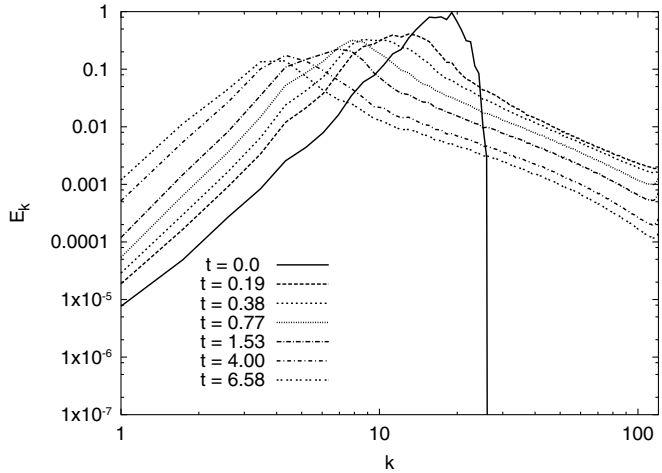

FIG. 11. The evolution of the magnetic-energy spectra in the viscous free-streaming regime ($R_e \ll 1$) for a magnetic field with maximal helicity. The simulations were performed on a mesh with 256^3 grid points, and the cutoff is $k_c \approx 16$.

atoms, do not respond to magnetic stresses and may therefore slip by the magnetic field lines, unless the scattering between neutral and charged particles is rapid enough. To investigate if this is the case one has to consider the (here assumed incompressible) equations of MHD with a significant neutral component

$$\varrho_{\rm i}\left(\frac{\partial \mathbf{v}_{\rm i}}{\partial t}+\mathbf{v}_{\rm i}\cdot\nabla\mathbf{v}_{\rm i}\right)=\frac{(\nabla\times\mathbf{B})\times\mathbf{B}}{4\pi}-\varrho_{\rm i}\alpha_{\rm in}(\mathbf{v}_{\rm i}-\mathbf{v}_{\rm n}), \tag{19}$$

$$\varrho_{\rm n}\left(\frac{\partial \mathbf{v}_{\rm n}}{\partial t}+\mathbf{v}_{\rm n}\cdot\nabla\mathbf{v}_{\rm n}\right)=-\varrho_{\rm n}\alpha_{\rm ni}(\mathbf{v}_{\rm n}-\mathbf{v}_{\rm i}), \tag{20}$$

where $\varrho_{\rm n}$, $\varrho_{\rm i}$, $\mathbf{v}_{\rm n}$, and $\mathbf{v}_{\rm i}$ are matter density and velocity of neutrals and ions, respectively, and we will assume $\varrho_{\rm i}\ll\varrho_{\rm n}$ throughout. The momentum transfer rates due to neutral-ion collisions satisfy

$$\alpha_{\rm ni}=\frac{\varrho_{\rm i}}{\varrho_{\rm n}}\alpha_{\rm in}\approx X_e\alpha_{\rm in}. \tag{21}$$

The equations of MHD are closed by including the induction equation

$$\frac{\partial\mathbf{B}}{\partial t}=\nabla\times(\mathbf{v}_{\rm i}\times\mathbf{B}) \tag{22}$$

for ions. The condition of tight coupling between ions and neutrals, i.e., $\mathbf{v}_D\equiv\mathbf{v}_{\rm i}-\mathbf{v}_{\rm n}\ll\mathbf{v}_{\rm i}$ may be derived from Eq. (20) (noting that the first two terms are usually of the same magnitude) to be equivalent to

$$\frac{\mathbf{v}_{\rm i}}{L}\approx\frac{\mathbf{v}_{\rm n}}{L}\ll X_e\alpha_{\rm in}. \tag{23}$$

One may show (cf. also [43–45]) self-consistently that in this limit the LHS of Eq. (19) is negligible, leaving the ion-neutral drift velocity v_D in the terminal velocity regime

$$\mathbf{v}_D=\frac{(\nabla\times\mathbf{B})\times\mathbf{B}}{4\pi\varrho_{\rm i}\alpha_{\rm in}}. \tag{24}$$

Inserting this equality into Eq. (20), and for $\mathbf{v}_{\rm n}\approx\mathbf{v}$, where $\mathbf{v}$ is the center-of-mass velocity, one obtains the usual Euler equation (1). The induction Eq. (22) is modified to include a dissipative term. Replacing $\mathbf{v}_{\rm i}=\mathbf{v}_D+\mathbf{v}_{\rm n}$ one finds

$$\frac{\partial\mathbf{B}}{\partial t}=\nabla\times(\mathbf{v}\times\mathbf{B})+\nabla\times\left(\frac{(\nabla\times\mathbf{B})\times\mathbf{B}}{4\pi\varrho_{\rm i}\alpha_{\rm in}}\times\mathbf{B}\right). \tag{25}$$

MHD of an ion-neutral mixture in the tightly coupled regime behaves thus as ordinary MHD with an additional dissipative term. The effect of this term may be estimated by defining an ambipolar Reynolds number as the comparison of the two terms on the RHS of Eq. (25), i.e.,

$$R_{\rm amb}\equiv\frac{vL\alpha_{\rm in}}{(v_{\rm A}^{\rm i})^2}\approx\frac{vL\alpha_{\rm in}X_e}{v_{\rm A}^2}, \tag{26}$$

where

$$v_{\rm A}^{\rm i}\approx v_{\rm A}/\sqrt{X_e} \tag{27}$$

is the Alfvén propagation velocity in the ion-neutral weakly coupled limit. It may be seen that the condition $R_{\rm amb}\gg 1$ (assuming self-consistently $v\sim v_{\rm A}$) automatically implies the tight-coupling condition Eq. (24). It is thus evident that MHD with dissipation due to ambipolar diffusion in the tight-coupling regime may never become viscous due to this ambipolar "drag" [46]. In the language (JKO98) appropriate to linear MHD this implies that overdamped modes proportional to the magnetic stresses do not exist. This is in stark contrast to MHD with fluid shear viscosity, or with momentum drag due to a homogeneous background component, where viscous MHD (i.e., overdamped modes) exist.

These arguments assume the absence of other sources of dissipation. Consider, for example, shear viscosity due to neutral-neutral scattering as described by a term $\varrho_{\rm n}\eta\nabla^2\mathbf{v}_{\rm n}$ on the RHS of Eq. (20). Assuming viscous MHD due to this term [i.e., the kinetic Reynolds number Eq. (4) $R_e\ll 1$] the condition for tight coupling is modified and now reads $\eta/L^2\ll\alpha_{\rm in}X_e$. Nevertheless, even in this case one finds that the condition of tight coupling is equivalent to the requirement $R_{\rm amb}\gg 1$. The flow may thus be viscous in the tight-coupling regime, but only due to sources of dissipation other than ambipolar diffusion.

Once the flows reach the limit $R_{\rm amb}\lesssim 1$ the neutral species decouples from the flow. In this limit MHD evolution is described by Eq. (19) with $v_{\rm n}\rightarrow 0$ and Eq. (22) completely analogous to MHD with free-streaming photons or neutrinos (cf. Sec. III) and with a Reynolds number given by Eq. (14). One may then show that the flow is viscous due to ambipolar drag. Only when $\alpha_{\rm in}$ is reduced by a further factor of $\sim\sqrt{X_e}$ (or equivalently, the Alfvén crossing time is reduced by the same factor) does turbulent MHD obtain again. When this happens typical fluid velocities are $v\approx v_{\rm A}^{\rm i}$, thus increased with respect to the tight-coupling regime.

It is important to stress the following. The system of equations (19), (20), and (22) provides only a proper description of MHD in the fluid limit when particle species have mean free paths much smaller than the scale under consideration. Whereas for the scales we consider (assuming magnetic fields not too weak) this may be the case for protons and electrons due to Coulomb scattering; this condition gets violated at late times for neutral particles. In this limit, i.e., $l_{\rm mfp}^{\rm n}\gg L$ mixing of neutrals from different regions becomes significant. Higher moments of the particle distribution $f_{\rm n}(x, v)$ (with the zeroth moment, density and the first, velocity) become significant such that a reduction of the Boltzmann equation to the Euler equation is not anymore adequate. When $l_{\rm mfp}^{\rm n}\gg L$ and $l_{\rm mfp}^{\rm i}\ll L$ one may nevertheless describe MHD by the fluid equations (19) and (22) for ions, and to a good

approximation, assume $\mathbf{v}_n \approx 0$ due to mixing of neutrals from different regions.

V. EVOLUTION OF COSMIC MAGNETIC FIELDS

In this section we present detailed analytical results for the evolution of subhorizon magnetic fields between an epoch of magnetogenesis (e.g., the electroweak transition at $T \approx 100$ GeV) and the much later onset of cosmic structure formation (at approximately redshift $z \approx 10$). Our analysis draws on the general results found in the previous sections, but includes viscosities as applicable in the early Universe. In particular, we give coherence length and energy density as functions of cosmic temperature, with generation epoch, magnetic spectral index, initial magnetic-energy density, and helicity left as free parameters. Though the results are fairly straightforward, when applied to the various regimes in the early Universe (i.e., turbulent and viscous due to photon and neutrino viscosities, respectively) a large number of expressions emerges. We therefore advise the more superficially interested reader to skip the third subsection of this section and proceed to the discussion of results in the next section.

A. Initial conditions

We define the Fourier transform of the magnetic fields such that the spatial average of magnetic field strength may be written as follows:

$$\langle B(x)^2 \rangle \equiv \int d\ln k \tilde{B}_k^2. \tag{28}$$

The spectrum of the magnetic field at the magnetogenesis epoch is parametrized by

$$\tilde{B}_{gc}(l_c) = \tilde{B}_{gc}(L_{gc})\left(\frac{l_c}{L_{gc}}\right)^{-n/2}. \tag{29}$$

Here, and in what follows, a subscript g denotes quantities at the magnetogenesis epoch and subscript c refers to *comoving* values. Here comoving lengths are defined as the lengths they would have at the present epoch [i.e., $l_c(T) = l(T)(a(T_0)/a(T))$ where a is the scale factor and T_0 presents cosmic temperature] and we define comoving field strength analogously as the field strength it would have at the present epoch, if the field would only evolve according to the requirement of flux conservation [i.e., $B_c(T) = B(T)(a(T)/a(T_0))^2$]. Note that $k = 2\pi/l$ and that whereas l denotes an arbitrary scale L always denotes the integral scale (k^I the integral wave vector), i.e., the energy containing, scale. Our analysis will focus on blue spectra $n > 0$ as appropriate for magnetic fields generated after an inflationary epoch by a causal process. Different magnetogenesis scenarios often have different proposed n. Since it is beyond the scope of the present paper to study magnetogenesis scenarios, we treat n as a free parameter with $n > 0$ to ensure a well-defined magnetic coherence length. We note, however, that $n = 3$ has been commonly proposed to result from the superposition of a large number of randomly oriented magnetic dipoles [36].

Given these definitions one may compute the magnetic field energy density at an arbitrary epoch as a function of the temperature dependent integral scale and the scale factor

$$\begin{aligned}\varrho_B(T) &= \left(\frac{a(T)}{a_0}\right)^4 \frac{1}{8\pi} \int_0^{k_c^I} d\ln k \tilde{B}_{gc}^2(L_{gc})\left(\frac{k_c(T)}{k_{gc}^I}\right)^n \\ &= \left(\frac{a(T)}{a_0}\right)^4 \frac{1}{8\pi n} \tilde{B}_{gc}^2(L_{gc})\left(\frac{L_c(T)}{L_{gc}}\right)^{-n}.\end{aligned} \tag{30}$$

It is convenient to define a ratio r between magnetic-energy density and a power of the total radiation entropy density

$$r \equiv \frac{\varrho_B}{s_r^{4/3}} \tag{31}$$

since for the constant comoving integral scale (i.e., no dynamic magnetic field evolution) this ratio stays constant with the expansion of the Universe. The dynamic (as opposed to geometric) evolution of the field is therefore more easily deduced from the evolution of r. The quantity r may be related to the ratio of magnetic field energy density and radiation energy density $r_\varrho = \varrho_B/\varrho_r$ by

$$r_\varrho = r\frac{4}{3}\left(\frac{2\pi^2}{45}\right)^{1/3} \frac{g_S^{4/3}}{g_r} \tag{32}$$

with g_S, g_r denoting statistical weight in entropy and radiation, respectively. Note here that r may be converted to average magnetic field strength

$$\begin{aligned}B(T) &= 5.72 \times 10^{-6}\ \mathrm{G} r^{1/2}(T)\left(\frac{g_S}{3.909}\right)^{4/3} \\ &\times \left(\frac{T}{2.351 \times 10^{-4}\ \mathrm{eV}}\right)^2\end{aligned} \tag{33}$$

such that the comoving (present day) magnetic field strength is $B_c = 5.72 \times 10^{-6}$ G for $r = 1$. (For $r_\gamma \equiv \varrho_B/\varrho_\gamma = 1$ the comoving field strength of $B_c = 3.24 \times 10^{-6}$ G results.) The magnetic field strength given in Eq. (33) yields an Alfvén velocity after the decoupling of photons of

$$\begin{aligned}v_A &= \frac{B}{\sqrt{4\pi\varrho}} \\ &= 8.86 \times 10^5 \frac{\mathrm{cm}}{\mathrm{s}}\left(\frac{r}{10^{-10}}\right)^{1/2}\left(\frac{\Omega_b h^2}{0.02}\right)^{-1/2}\left(\frac{T}{0.259\ \mathrm{eV}}\right)^{1/2},\end{aligned} \tag{34}$$

where $g_S = 3.909$ has been assumed and with $\varrho = \varrho_b$ in the fully ionized case before recombination as well as in the partially ionized case in the tightly coupled regime

after recombination (cf. Sec. IV). Here ϱ_b and Ω_b denote baryonic density and fractional contribution to the critical density at the present epoch whereas h is the Hubble constant in units of $100\,\mathrm{km\,s^{-1}\,Mpc^{-1}}$. We alert the reader to the distinction between decoupling of photons (i.e., $l_\gamma \gtrsim L$) (typically occurring before recombination) and recombination itself. Equation (34) may be compared to the plasma speed of sound

$$v_b = \sqrt{\gamma \frac{T_b}{m_b}} = 5.99 \times 10^5 \frac{\mathrm{cm}}{\mathrm{s}} \gamma^{1/2} \left(\frac{T_b}{0.259\ \mathrm{eV}}\right)^{1/2}, \quad (35)$$

where $\gamma = 10/3$ and 2 for adiabatic and isothermal compression, respectively, and where we have neglected corrections due to the presence of helium. Note that below redshift $z \lesssim 100$ the baryon temperature falls more rapidly than the photon temperature, i.e., as $T_b \sim a^{-2}$.

To determine the integral scale at the generation epoch, L_g, we assume that turbulence pertains, such that L_g is obtained by setting the Hubble rate at the generation epoch equal to the Alfvén eddy-turnover rate. This yields

$$L_{gc} \equiv L_c(T_g) = \left(\frac{2025}{4\pi^7}\right)^{1/6} \frac{M_{\mathrm{Pl}}}{T_0 T_g} g_{S0}^{-1/3} \sqrt{n r_g} \quad (36)$$

$$\simeq 1.55 \times 10^{-4}\ \mathrm{pc} \sqrt{n} \left(\frac{r_g}{0.01}\right)^{1/2} \left(\frac{T_g}{100\ \mathrm{GeV}}\right)^{-1}, \quad (37)$$

where $M_{\mathrm{Pl}} = 1/\sqrt{G} \approx 1.22 \times 10^{19}\ \mathrm{GeV}$ is the Planck mass. In the above, the subscript 0 denotes quantities evaluated at the present epoch. Finally, we parametrize initial helicity of the field by a dimensionless number h_g

$$\mathcal{H}_{gc} = h_g \mathcal{H}^{gc}_{\mathrm{max}}, \quad \text{with } \mathcal{H}^{gc}_{\mathrm{max}} \approx \frac{2\pi}{n-1} \tilde{B}^2_{gc}(L_{gc}) L_{gc} \quad (38)$$

such that $h_g \leq 1$.

B. Evolution: The general picture

The evolution of a stochastic magnetic field in the early Universe is described by alternating epochs of turbulent MHD and viscous MHD. Here the latter epochs occur when viscosities due to neutrinos, or photons, become significant. Such a picture has already been established by JKO98. With the assumed blue magnetic spectra, the gross features of the magnetic field evolution are described by the growth of the integral scale. Following the arguments in Sec. II the instantaneous integral scale is given by the equality between cosmic time and eddy-turnover time at the scale L

$$\frac{1}{t_{\mathrm{eddy}}} \approx \frac{v(L)}{L_p(T)} \approx H(T) \approx \frac{1}{t_H} \quad (39)$$

holding equally for turbulent and viscous eras. In the above expression the subscript p denotes the proper (as opposed to comoving) value of the integral scale, $v(L)$ is the fluid velocity on scale L, and H is the Hubble parameter. The velocities v may be determined from the Euler equation [Eq. (1)] by an approximate balance of either the second and third terms on the LHS in the turbulent case ($R_e > 1$) or the third term on the LHS and the dissipation term on the RHS in the viscous case. This yields

$$v(L) \approx v_{\mathrm{A}}(L); \qquad R_e > 1 \quad (40)$$

in the turbulent case and

$$v(L) \approx \frac{v_{\mathrm{A}}^2(L) L}{\eta}, \qquad v(L) \approx \frac{v_{\mathrm{A}}^2(L)}{\alpha L}, \qquad R_e < 1 \quad (41)$$

in the photon (neutrino) diffusive and free-streaming viscous cases, respectively. Note that the velocities in the viscous case may also be written in a unifying way as $v(L) \approx R_e v_{\mathrm{A}}$ with $R_e < 1$ the Reynolds number Eq. (4) evaluated with the Alfvén velocity, i.e., $v = v_{\mathrm{A}}$.

Equation (39) is to be evaluated with proper quantities. Since a given scale expands continuously with the Universe, i.e., $l_p = a l_c$, the eddy-turnover (relaxation) time on this scale increases with the expansion of the Universe. This relaxation time increase is enhanced after the decoupling of photons by an additional decrease of the Alfvén velocity, i.e., $v_{\mathrm{A}} \propto B(T)/\sqrt{4\pi\varrho_b} \propto a^{-1/2}$ (whereas, $v_{\mathrm{A}} \propto a^0$ when photons are still coupled to the MHD evolution). On the other hand, the Hubble time increases as $t_H \propto a^2$ during radiation domination (RD) and as $\propto a^{3/2}$ during matter domination (MD). During turbulent evolution, the combined effect is such

$$\frac{t_{\mathrm{eddy}}}{t_H} \approx \frac{L/v_{\mathrm{A}}}{t_H} \propto \frac{a}{a^2} \propto 1/a \quad \text{(RD)}$$
$$\propto \frac{a/1/a^{1/2}}{a^{3/2}} \propto a^0 \quad \text{(MD)} \quad (42)$$

that during RD larger and larger scales may be processed, i.e., that the comoving integral scale L_c may grow as the Universe expands. In contrast, during MD the ratio between eddy and Hubble time stays constant, permitting only logarithmic growth of L_c. This, however, is only the case while the fluid is turbulent. For sufficiently strong fields (see below) turbulence recommences right after recombination, with the fluid before recombination strongly dragged by free-streaming photons. In the viscous regime, with viscosity provided by photons, one finds $\eta_\gamma \propto a^3$ and $\alpha_\gamma \propto a^{-4}$ (cf. Appendix C). This yields for the comparison of time scales

$$\frac{t_{\mathrm{eddy}}}{t_H} \approx \frac{L/v}{t_H} \propto a \quad \text{(photon diffusion)}$$
$$\propto a^{-5/2} \quad \text{(photon free streaming)}, \quad (43)$$

where we have assumed radiation domination during the

diffusive regime and matter domination during the free-streaming regime. It may be seen from Eq. (43) that the integral scale may further increase during the viscous MHD regime when photons are free streaming. On the other hand, one may show quite generally that an increase during the photon diffusion regime is always prohibited. Essentially identical conclusions result in the case of neutrinos.

The following general picture for the evolution of the integral scale thus emerges. At early times, close to the epoch of magnetogenesis in the early Universe, the fluid is turbulent and as the Universe expands the comoving scale where one eddy turnover is possible in cosmic time is continuously increasing. By the process of a direct cascade the energy of this (integral) scale L_c may thus be dissipated, leaving only the tail of the initial magnetic field at scales larger than the integral scale. The spectrum of the magnetic field is thus described by

$$\tilde{B}_c(l_c) = \tilde{B}_{gc}(L_{gc})\left(\frac{l_c}{L_{gc}}\right)^{-n/2}, \qquad l_c \geq L_c. \tag{44}$$

As the Universe cools down shear viscosity due to neutrinos becomes large, thereby reducing the Reynolds number of the flow. At the epoch when the Reynolds number becomes of order unity on the integral scale, a regime of viscous MHD commences. At this point, a further increase of L_c is prohibited, since in the diffusive regime the relaxation time grows more rapid than the Hubble time. Any existing fluid flows are dissipated, leaving, nevertheless, the magnetic field at scales beyond $L^{\nu}_{\rm EOT}$ intact. Here $L^{\nu}_{\rm EOT}$ refers to the integral scale when $R_{e\nu}(L(T_{\rm EOT}))$ has decreased to unity. This is analogous to the survival of magnetic fields in the overdamped regime of linearized modes, as discussed in JKO98. Only some time after neutrinos have decoupled from the fluctuations, i.e., when $l_\nu \gg L$, the integral scale may grow beyond that given at the epoch of the end of turbulence, $L^{\nu}_{\rm EOT}$. During this dissipation of magnetic fields in the viscous free-streaming regime, the integral scale grows more rapidly then during the turbulent regime. This more rapid increase (as opposed to a slower increase in the nonexpanding case, cf. Sec. III) is mainly due to the strong temperature dependence of the drag term. Since the neutrino drag is continuously decreasing, some time before neutrino decoupling at $T \approx 2.6$ MeV the fluid enters again a turbulent stage. At this point, the integral scale has grown to a value, as if the plasma would have not at all gone through a viscous period. The viscous period thus just delays the dissipation of magnetic fields. These evolutionary trends are shown in Figs. 12–15, which show the growth of magnetic coherence length, and the decay of magnetic-energy density, for a number of initial conditions. The evolution of the kinetic Reynolds number R_e is also shown for a particular scenario. The frozen-in state of magnetic fields during the

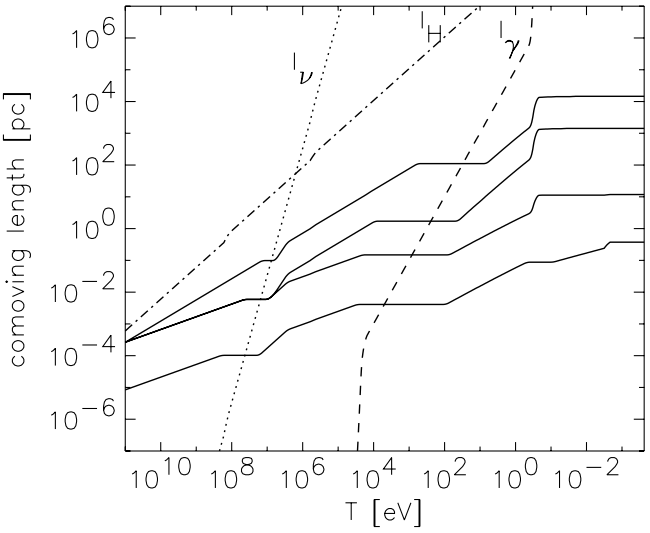

FIG. 12. The evolution of comoving coherence length for initial magnetic field configurations with different spectral indices n and initial magnetic helicities. Solid lines from top to bottom: (*a*) $h_g = 1$, $r_g = 0.01$; (*b*) $h_g = 10^{-3}$, $n = 3$, $r_g = 0.01$; (*c*) $h_g = 0$, $n = 3$, $r_g = 0.01$; (*d*) $h_g = 0$, $n = 3$, $r_g = 10^{-5}$. The labels l_ν, l_γ, and $l_{\rm H}$ refer to the comoving mean free paths of neutrinos and photons and the comoving Hubble length, respectively. The epoch of magnetogenesis was assumed to occur during the electroweak phase transition ($T_g = 100$ GeV).

diffusive neutrino regime with $R_e \lesssim 1$ and the first part of the free-streaming neutrino regime becomes apparent by the plateaus in L_c one finds at $T \sim 10^7$–10^8 eV.

A similar picture results for magnetic field evolution after neutrino decoupling, but now with neutrinos replaced by photons. There are, however, subtle differences.

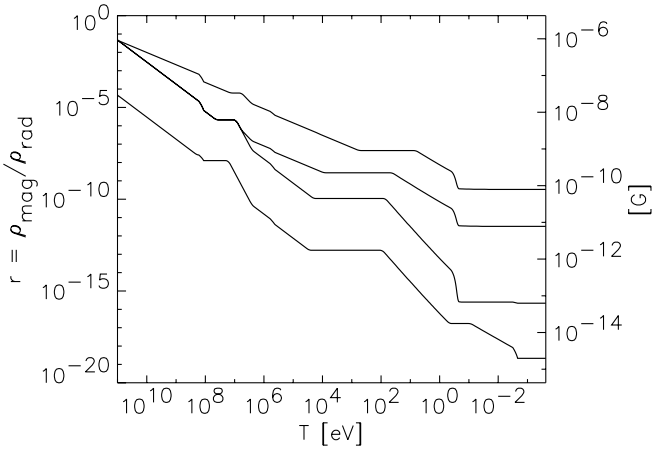

FIG. 13. The evolution of the relative magnetic-energy density r corresponding to the models shown in Fig. 12. Solid lines from top to bottom: (*a*) $h_g = 1$, $r_g = 0.01$; (*b*) $h_g = 10^{-3}$, $n = 3$, $r_g = 0.01$; (*c*) $h_g = 0$, $n = 3$, $r_g = 0.01$; (*d*) $h_g = 0$, $n = 3$, $r_g = 10^{-5}$. The epoch of magnetogenesis was assumed to occur during the electroweak phase transition ($T_g = 100$ GeV).

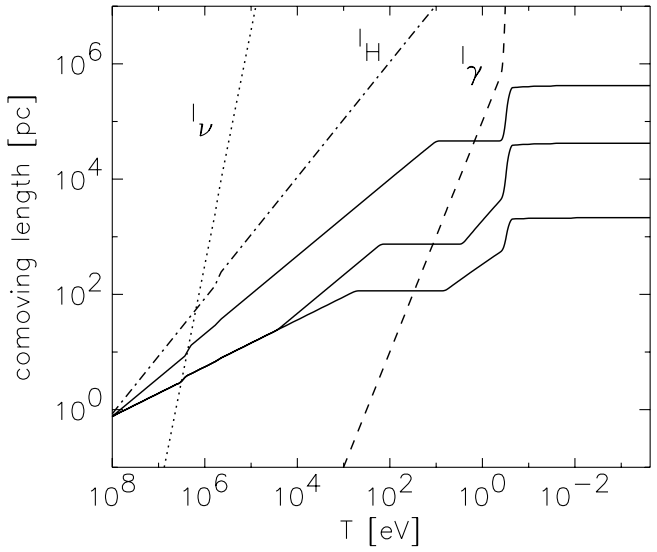

FIG. 14. The evolution of comoving coherence length for different initial magnetic field configurations. Solid lines from top to bottom: (*a*) $h_g = 1$, $r_g = 0.083$, $n = 3$; (*b*) $h_g = 10^{-3}$, $r_g = 0.083$, $n = 3$; (*c*) $h_g = 0$, $r_g = 0.083$, $n = 3$. The labels l_ν, l_γ, and $l_{\rm H}$ refer to the comoving mean free paths of neutrinos and photons and the comoving Hubble length, respectively. The epoch of magnetogenesis was assumed to occur during the QCD phase transition ($T_g = 100$ MeV).

After the electrons and positrons become nonrelativistic, i.e., $T < m_e$, the photon mean free path increases rapidly. This is particularly true during the period of the $e^\pm$ annihilation, i.e., $500 \gtrsim T \gtrsim 20$ keV [47]. Therefore, viscous MHD evolution with photons diffusing commences for a wide parameter space during this period. The epoch of viscous MHD with drag provided by free-streaming

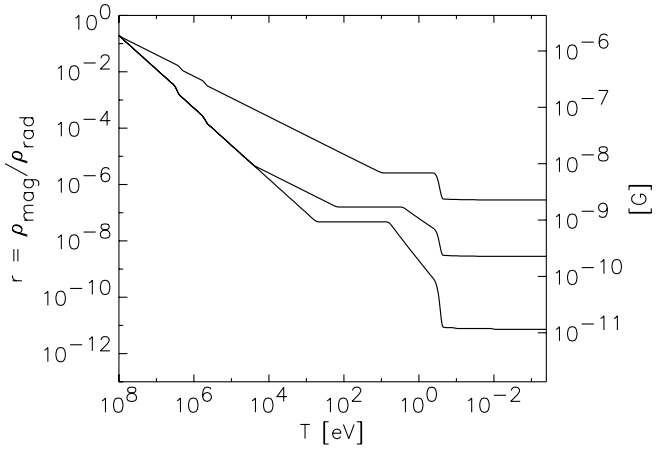

FIG. 15. The evolution of the relative magnetic-energy density r corresponding to the models shown in Fig. 14. Solid lines from top to bottom: (*a*) $h_g = 1$, $r_g = 0.083$, $n = 3$; (*b*) $h_g = 10^{-3}$, $r_g = 0.083$, $n = 3$; (c) $h_g = 0$, $r_g = 0.083$, $n = 3$. The epoch of magnetogenesis was assumed to occur during the QCD phase transition ($T_g = 100$ MeV).

photons, which starts some time later, is always ended right at recombination ($T \approx 0.26$ eV). This, of course, is due to the virtually instantaneous decrease of α_γ by a factor $\sim 10^4$ which is the result of the loss of free electrons during recombination. In contrast to dissipation due to neutrinos, the viscous period due to photons thus does not only simply delay the growth of the integral scale (i.e., the dissipation). Rather, shortly before the end of the viscous MHD regime before recombination magnetic field strengths are genuinely larger and integral scales are smaller as compared to a scenario where the flow would have stayed turbulent all along. What happens after recombination depends then on the strength of the magnetic field at recombination.

After recombination two different potential sources of dissipation come into play; ambipolar diffusion as well as shear viscosity due to hydrogen atoms. We assume, for the moment, a turbulent flow, i.e., $v \approx v_{\rm A}$, with resulting conclusions turning out independent of this assumption. With the aid of Eq. (39), evaluated shortly after recombination, one may determine the ambipolar Reynolds number Eq. (26) to be approximately $R_{\rm amb} \approx 10^4$. It follows that the hydrogen atoms are tightly coupled to the flow (cf. Sec. IV). As this is the case, viscosity due to neutrals may play a role. One may evaluate the kinetic Reynolds number R_e Eq. (4) on the integral scale at recombination due to hydrogen viscosity by noting that the Alfvén crossing rate on the integral scale shortly before recombination $(v_{\rm A}/L)_{\rm rec}$ is given by $(\sqrt{\alpha_\gamma H})_{\rm rec}$ [cf. Eqs. (39) and (41) applied in the viscous photon-free-streaming regime shortly before recombination]. When this is done one finds that weak magnetic fields with small coherence lengths [48] are entering a viscous regime due to hydrogen viscosity immediately after recombination, whereas strong fields do not. Here, the dividing magnetic field strength is given approximately by $B_c^\eta \approx 10^{-13}$ G, corresponding to integral scales $L_c \approx 10$ pc (cf. Figs. 12 and 13). Thus, fields with $B_c \lesssim B_c^\eta$ are not significantly processed immediately after recombination. Only some time later, when neutrals have decoupled from the flow, they are subject to further processing (i.e., increase of coherence length). This further increase in L mostly takes place at epochs with redshift $z \lesssim 100$. The increase in integral scale then occurs in a viscous regime with drag due to free-streaming hydrogen atoms (cf. Sec. IV), quite analogous to the regime shortly before recombination. The flows become turbulent again only when the Universe is reionized as ambipolar drag then disappears [49]. The epoch of reionization occurs presumably at $z \simeq 10$, at which point the integral scale grows virtually instantaneous to a larger value and stays approximately constant thereafter [50].

In contrast, fields with strength $B \gtrsim B_c^\eta$ recommence turbulence after recombination. The growth of the coher-

ence scale during the recombination epoch is characterized by an almost instantaneous increase of a factor of order ~5, associated with dissipation into heat. Subsequent evolution only increases the integral scale at best logarithmically, due to the peculiar redshifting of Alfvén crossing time and Hubble constant [cf. Eq. (42)]. One may show that even such fields enter a viscous period later on, with viscosity first due to diffusing hydrogens in the tight-coupling regime and later due to ion-hydrogen collisions (ambipolar drag) in the weak ion-hydrogen coupling limit. In any case, the magnetic coherence scale is not modified much anymore, even after the epoch of reionization [51]. Again, these trends may be followed in Figs. 12–15.

We have so far assumed that magnetic helicity is negligible. Because of the high Prandtl numbers in the early Universe helicity is conserved. Since for typical blue spectra with $n > 1$ nonhelical fields decay more rapidly than helical fields (cf. Sec. II), and initial fields with submaximal helicity $h_g < 1$ will ultimately reach a maximally helical configuration during the course of field dissipation. Somewhat oversimplifying it may be understood as the nonhelical component dissipating leaving the fully helical component as a remnant. There exists a simple criterion of when the fully maximal case is reached. Using Eqs. (29) and (38) and the assumption of initial nonhelical evolution, one may show that maximal helicity is reached when the integral scale has grown to

$$L_c^{\max} = L_{gc} h_g^{-1/(n-1)}. \tag{45}$$

The subsequent evolution of the field is different from the nonhelical case. Whereas processing (i.e., cascading of energy to smaller scales) on the integral scale and the growth thereof still proceeds according to the requirement Eq. (39), the required inverse cascade due to the conservation of helicity implies a transfer of energy from small scales to large scales. The instantaneous magnetic field spectrum is thus modified compared to Eq. (29) and given by

$$\tilde{B}_c(l_c) = \tilde{B}_{gc}(L_{gc}) h_g^{1/2} \left(\frac{L_c(T)}{L_{gc}}\right)^{(n-1)/2} \left(\frac{l_c}{L_{gc}}\right)^{-n/2} \qquad l_c \geq L_c. \tag{46}$$

Note that, in contrast to Eq. (44), the prefactor of this spectrum is time dependent (through the temperature dependence of L_c). In accordance with the findings of Sec. II, the spectrum retains its initial slope n on scales $l_c \geq L_c$. It may be noted that due to the large dynamic increase of $L_c(T)$ between magnetogenesis and recombination, even fields with initially very small helicity typically have reached maximal helicity by recombination.

C. Evolution: Analytic results

As discussed above, and observed in Figs. 12 and 14, the growth of the integral scale before recombination takes place in different regimes, i.e., turbulent MHD with neutrino viscosity, viscous MHD with free-streaming neutrinos, turbulent MHD with photon viscosity, and viscous MHD with free-streaming photons. Moreover, it is dependent on whether maximal helicity has been reached or not. After recombination strong magnetic fields ($B_c > B_c^{\eta}$) undergo only a slight further evolution in the turbulent regime, whereas weaker magnetic fields may pass through an extended viscous hydrogen free-streaming regime.

In the following we give analytic results for the integral scale and energy density in the different regimes, expressed as functions of the initial conditions. Here most (but not all) of the notation should be clear from the definitions in prior sections (e.g., subscripts of r, S, f, l, q, ν, γ, b, and p indicate, total radiation, entropy, particles coupled to the fluid, leptons, quarks, neutrinos, photons, baryons, and protons, respectively, whereas a subscript 0 denotes quantities at the present epoch). One may in principle also derive the transition temperatures, $T_{\rm EOT}$ and $T_{\rm EOV}$, at which the fluid passes from a turbulent state into a viscous one, and vice versa, defined by $R_e \approx 1$. We have nevertheless refrained from doing so, as the number of expressions quickly exponentiates, and in some circumstances (i.e., $0.5\ {\rm MeV} \gtrsim T \gtrsim 20\ {\rm keV}$ due to the $e^{\pm}$ annihilation) closed forms may not be derived.

1. Evolution before neutrino decoupling

The expressions for the integral scale and energy density during turbulent MHD evolution before neutrino decoupling are identical to those before recombination. The reader is thus referred to Eqs. (54) and (55), for the case of submaximally helical fields, and to (58) and (59), for maximally helical fields. The expressions for L_c and r in the viscous neutrino free-streaming regime, for submaximally helical (i.e., $L_c < L_c^{\max}$) fields are

$$L_c(T) = L_{gc}\left[G_1\left(\frac{1}{G_F^2 M_{\rm pl} T_g^3}\right)\right]^{1/(2+n)} \left(\frac{T}{T_g}\right)^{-5/(2+n)}, \tag{47}$$

$$r(T) = r_g\left[G_1\left(\frac{1}{G_F^2 M_{\rm pl} T_g^3}\right)\right]^{-n/(2+n)} \left(\frac{T}{T_g}\right)^{5n/(2+n)}, \tag{48}$$

with

$$G_1 \equiv \frac{1}{\zeta(3)}\left(\frac{49\pi^7}{405}\right)^{1/2} \frac{g_r^{5/2}}{g_f g_\nu (g_l + g_q)}. \tag{49}$$

Here L_{gc} is given in Eq. (37). As a numerical example, with index $n = 3$ and $g_r = 10.75$, $g_f = 5.5$, $g_\nu = 5.25$, $g_l = 3.5$, and $g_q = 0$ as applicable between QCD transition and neutrino decoupling one finds

$$L_c(T) \simeq 2.1 \times 10^{-2}\ \mathrm{pc}\left(\frac{r_g}{0.01}\right)^{1/2}\left(\frac{T_g}{100\ \mathrm{GeV}}\right)^{-3/5} \times \left(\frac{T}{2.6\ \mathrm{MeV}}\right)^{-1}, \quad (50)$$

$$r(T) \simeq 2.1 \times 10^{-8}\left(\frac{r_g}{0.01}\right)\left(\frac{T_g}{100\ \mathrm{GeV}}\right)^{-6/5}\left(\frac{T}{2.6\ \mathrm{MeV}}\right)^{3}. \quad (51)$$

For maximally helical fields (i.e., $L > L_c^{\max}$) the appropriate expressions are found from Eqs. (47) and (48) by replacing $n \rightarrow 1$, except in L_{gc}^I which leaves a $\sqrt{n}$ dependence in L_c, as well as multiplying the RHS of Eq. (47) by $h_g^{1/3}$ and the RHS of Eq. (48) by $h_g^{2/3}$. This yields the following numerical examples:

$$L_c(T) \simeq 4.8 \times 10^{-2}\ \mathrm{pc}\sqrt{n}\left(\frac{r_g}{0.01}\right)^{1/2}\left(\frac{h_g}{0.01}\right)^{1/3} \times \left(\frac{T_g}{100\ \mathrm{GeV}}\right)^{-1/3}\left(\frac{T}{2.6\ \mathrm{MeV}}\right)^{-5/3}, \quad (52)$$

$$r(T) \simeq 3.2 \times 10^{-7}\left(\frac{r_g}{0.01}\right)\left(\frac{h_g}{0.01}\right)^{2/3}\left(\frac{T_g}{100\ \mathrm{GeV}}\right)^{-2/3} \times \left(\frac{T}{2.6\ \mathrm{MeV}}\right)^{5/3}, \quad (53)$$

where the same parameters as above have been assumed.

2. Evolution before recombination

The integral scale and magnetic energy during MHD turbulence $R_e > 1$ (equally applicable before neutrino coupling and recombination) before maximal helicity has been reached (i.e., for $L_c < L_c^{\max}$) read

$$L_c(T) = L_{gc}\left(\frac{g_S}{g_r^{1/2}g_f^{1/2}}\right)^{2/(2+n)}\left(\frac{T}{T_g}\right)^{-2/(2+n)} = \left(\frac{2025}{4\pi^7}\right)^{1/6}\sqrt{n r_g}\,\frac{M_{\mathrm{Pl}}}{T_g T_0}\,g_{S0}^{-1/3}\left(\frac{g_S}{g_r^{1/2}g_f^{1/2}}\right)^{2/(2+n)} \times \left(\frac{T}{T_g}\right)^{-2/(2+n)}, \quad (54)$$

$$r(T) = r_g\left(\frac{g_S}{g_r^{1/2}g_f^{1/2}}\right)^{-2n/(2+n)}\left(\frac{T}{T_g}\right)^{2n/(2+n)}. \quad (55)$$

A numerical example for $n = 3$, $g_r = 3.36$, $g_f = 2$, and $g_S = 3.909$ as applicable after the $e^{\pm}$ annihilation is given by

$$L_c(T) \simeq 8.0 \times 10^{-2}\ \mathrm{pc}\left(\frac{r_g}{0.01}\right)^{1/2}\left(\frac{T_g}{100\ \mathrm{GeV}}\right)^{-3/5} \times \left(\frac{T}{100\ \mathrm{keV}}\right)^{-2/5}, \quad (56)$$

$$r(T) \simeq 3.9 \times 10^{-10}\left(\frac{r_g}{0.01}\right)\left(\frac{T_g}{100\ \mathrm{GeV}}\right)^{-6/5}\left(\frac{T}{100\ \mathrm{keV}}\right)^{6/5}. \quad (57)$$

Similarly, when maximal helicity has been reached $L_c > L_c^{\max}$ (essentially using the above equations with $n \rightarrow 1$ replaced and inclusion of h_g factors as in the preceding section) one finds

$$L_c(T) = L_{gc}\left(\frac{g_S}{g_r^{1/2}g_f^{1/2}}\right)^{2/3}\left(\frac{T}{T_g}\right)^{-2/3}h_g^{1/3}, \quad (58)$$

$$r = r_g\left(\frac{g_S(T)}{g_r^{1/2}g_f^{1/2}}\right)^{-2/3}\left(\frac{T}{T_g}\right)^{2/3}h_g^{2/3}. \quad (59)$$

A numerical example for $g_r = 3.36$, $g_f = 2$, and $g_S = 3.909$ is given by

$$L_c(T) \simeq 4.4 \times 10^{-1}\ \mathrm{pc}\sqrt{n}\left(\frac{r_g}{0.01}\right)^{1/2}\left(\frac{h_g}{0.01}\right)^{1/3} \times \left(\frac{T_g}{100\ \mathrm{GeV}}\right)^{-1/3}\left(\frac{T}{100\ \mathrm{keV}}\right)^{-2/3}, \quad (60)$$

$$r(T) \simeq 3.5 \times 10^{-8}\left(\frac{r_g}{0.01}\right)\left(\frac{h_g}{0.01}\right)^{2/3}\left(\frac{T_g}{100\ \mathrm{GeV}}\right)^{-2/3} \times \left(\frac{T}{100\ \mathrm{keV}}\right)^{2/3}, \quad (61)$$

which is virtually independent of the spectral index n. The expressions during viscous MHD with free-streaming photons (where we assumed $T < 20$ keV as is usually the case) for $L_c < L_c^{\max}$ are

$$L_c(T) = L_{gc}\left[G_2\frac{T_0}{M_{\mathrm{pl}}}\frac{T_0}{\sigma_{\mathrm{T}}n_{b0}X_e}\frac{T_0}{T_g}\right]^{1/(2+n)}\left(\frac{T_g}{T}\right)^{3/(2+n)}, \quad (62)$$

$$r(T) = r_g\left[G_2\frac{T_0}{M_{\mathrm{pl}}}\frac{T_0}{\sigma_{\mathrm{T}}n_{b_0}X_e}\frac{T_0}{T_g}\right]^{-n/(2+n)}\left(\frac{T}{T_g}\right)^{3n/(2+n)}, \quad (63)$$

with

$$G_2 \equiv \left(\frac{\pi^3}{45}\right)^{1/2}g_S^2 g_r^{-1/2}R_r^{1/2}, \quad (64)$$

and where $\sigma_{\mathrm{T}} = 8\pi\alpha^2/3m_e^2 \approx 6.65 \times 10^{-25}\ \mathrm{cm}^2$ is the Thomson cross section. Here, $R_r \equiv \varrho_r/(\varrho_r + \varrho_{\mathrm{DM}})$ accounts for a significant contribution of dark matter to the Hubble expansion shortly before recombination and X_e is the ionization fraction ($X_e \approx 1$ before recombination and $X_e \approx 10^{-4}$ after). As a numerical example for $n = 3$, $\Omega_b h^2 = 0.02$, and $X_e = 1$ one finds

$$L_c(T) \simeq 4.0\ \mathrm{pc}\left(\frac{r_g}{0.01}\right)^{1/2}\left(\frac{R_r}{0.235}\right)^{1/10}\left(\frac{T_g}{100\ \mathrm{GeV}}\right)^{-3/5} \times \left(\frac{T}{0.259\ \mathrm{eV}}\right)^{-3/5}, \quad (65)$$

$$r(T) \simeq 3.1 \times 10^{-15}\left(\frac{r_g}{0.01}\right)\left(\frac{R_r}{0.235}\right)^{-3/10}\left(\frac{T_g}{100\ \mathrm{GeV}}\right)^{-6/5} \times \left(\frac{T}{0.259\ \mathrm{eV}}\right)^{9/5}, \quad (66)$$

where $T \simeq 0.259$ eV corresponds to the temperature at recombination and $R_r \simeq 0.235$ for $\Omega_{\mathrm{tot}}h^2 = 0.15$. Similarly, for maximally helical fields $L > L^h_{\mathrm{max}}$ one finds the analytic expressions from those for the submaximal case, as above, by simply replacing in Eqs. (62) and (63) $n \rightarrow 1$, except in L_{gc}, as well as adding a factor $h_g^{1/3}$ in Eq. (62) and a factor $h_g^{2/3}$ in Eq. (63). Numerical examples are given by

$$L_c(T) \simeq 0.3\ \mathrm{kpc}\sqrt{n}\left(\frac{r_g}{0.01}\right)^{1/2}\left(\frac{h_g}{0.01}\right)^{1/3}\left(\frac{R_r}{0.235}\right)^{1/6} \times \left(\frac{T_g}{100\ \mathrm{GeV}}\right)^{-1/3}\left(\frac{T}{0.259\ \mathrm{eV}}\right)^{-1}, \quad (67)$$

$$r(T) \simeq 5.2 \times 10^{-11}\left(\frac{r_g}{0.01}\right)\left(\frac{h_g}{0.01}\right)^{2/3}\left(\frac{R_r}{0.235}\right)^{-1/6} \times \left(\frac{T_g}{100\ \mathrm{GeV}}\right)^{-2/3}\left(\frac{T}{0.259\ \mathrm{eV}}\right). \quad (68)$$

3. Evolution after recombination

In the turbulent regime after recombination the quantities of interest for $L_c < L_c^{\mathrm{max}}$ are given by

$$L_c = L_{gc}\left[\frac{\Omega_\gamma}{\sqrt{3\Omega_{\mathrm{tot}}\Omega_b}}\, g_{S0}\ln(a/a_{\mathrm{rec}})\right]^{2/(2+n)}\left(\frac{T_g}{T_0}\right)^{2/(2+n)}, \quad (69)$$

$$r = r_g\left[\frac{\Omega_\gamma}{\sqrt{3\Omega_{\mathrm{tot}}\Omega_b}}\, g_{S0}\ln(a/a_{\mathrm{rec}})\right]^{-2n/(2+n)}\left(\frac{T_0}{T_g}\right)^{2n/(2+n)}, \quad (70)$$

including a mild logarithmic growth factor $\ln(a/a_{\mathrm{rec}})$. Here Ω_γ, Ω_b, and Ω_{tot} are the present day fractional contributions to the critical density of CMBR photons, baryons, and total matter, respectively. (In the derivation of this expression the contribution of radiation to the total density after recombination has been neglected. This induces about $\sim$10% error in r and 5% in L_c immediately at recombination for the values below, but is asymptotically correct.) Numerical examples for $n = 3$, $g_{S0} = 3.909$, $\Omega_{\mathrm{tot}}h^2 = 0.15$, $\Omega_b h^2 = 0.02$, and $\Omega_\gamma h^2 = 2.48 \times 10^{-5}$ are

$$L_c(T) \simeq 12\ \mathrm{pc}\left(\frac{r_g}{0.01}\right)^{1/2}\left(\frac{T_g}{100\ \mathrm{GeV}}\right)^{-3/5}, \quad (71)$$

$$r(T) \simeq 1.1 \times 10^{-16}\left(\frac{r_g}{0.01}\right)\left(\frac{T_g}{100\ \mathrm{GeV}}\right)^{-6/5}, \quad (72)$$

$$B_c(T) \simeq 6.0 \times 10^{-14}\ \mathrm{G}\left(\frac{r_g}{0.01}\right)^{1/2}\left(\frac{T_g}{100\ \mathrm{GeV}}\right)^{-3/5}, \quad (73)$$

where we have also evaluated the comoving field strength via Eq. (33). For the above quantities we neglected the factor $\ln(a/a_{\mathrm{rec}})$ (as for most fields the period of turbulent MHD after recombination is rather short), Similarly, for $L > L^h_{\mathrm{max}}$ (when having attained maximal helicity) one finds

$$L_c = L_{gc}\left[\frac{\Omega_\gamma}{\sqrt{3\Omega_{\mathrm{tot}}\Omega_{\mathrm{b}}}}\, g_{S0}\ln(a/a_{\mathrm{rec}})\right]^{2/3}\left(\frac{T_g}{T_0}\right)^{2/3} h_g^{1/3}, \quad (74)$$

$$r = r_g\left[\frac{\Omega_\gamma}{\sqrt{3\Omega_{\mathrm{tot}}\Omega_{\mathrm{b}}}}\, g_{S0}\ln(a/a_{\mathrm{rec}})\right]^{-2/3}\left(\frac{T_0}{T_g}\right)^{2/3} h_g^{2/3}, \quad (75)$$

with numerical examples (with the input numerical values as above) given by

$$L_c(T) \simeq 1.9\ \mathrm{kpc}\sqrt{n}\left(\frac{r_g}{0.01}\right)^{1/2}\left(\frac{h_g}{0.01}\right)^{1/3}\left(\frac{T_g}{100\ \mathrm{GeV}}\right)^{-1/3}, \quad (76)$$

$$r(T) \simeq 8.1 \times 10^{-12}\left(\frac{r_g}{0.01}\right)\left(\frac{h_g}{0.01}\right)^{2/3}\left(\frac{T_g}{100\ \mathrm{GeV}}\right)^{-2/3}, \quad (77)$$

$$B_c(T) \simeq 1.6 \times 10^{-11}\ \mathrm{G}\left(\frac{r_g}{0.01}\right)^{1/2}\left(\frac{h_g}{0.01}\right)^{1/3} \times \left(\frac{T_g}{100\ \mathrm{GeV}}\right)^{-1/3}. \quad (78)$$

Note that there is only a residual dependence on spectral index n.

VI. SUMMARY AND DISCUSSION

The detailed numerical and analytical examination presented in the previous chapters has led to a surprisingly simple picture concerning the gross features of cosmic magnetic field evolution, in particular, the evolution of magnetic coherence scale and energy density. The growth of the coherence scale is described by the simple *causality* relation

$$v(L)/L \approx H(T) \quad (79)$$

independent if occurring in high kinetic Reynolds number $R_e \gg 1$ turbulent flow with $v \approx v_{\mathrm{A}}$ or during the multiple epochs of viscous ($R_e \ll 1$) MHD evolution with $v \ll v_{\mathrm{A}}$ [with v given by Eq. (41)] and independent

of the helical properties of the fields. In particular, nonlinear (direct) cascading of magnetic energy to the dissipation scale always occurs on that scale. Remaining magnetic-energy densities after evolution from very high temperature to an epoch with temperature T are then simply given, in the submaximal case, by all the initial magnetic energy present on scales $l \gtrsim L^{>}$, with $L^{>}$ the as yet largest length scale having been processed during prior evolution, and in the maximally helical case, by conservation of helicity density [see Eq. (10)] with the field sitting on scales $l \gtrsim L^{>}$. Quantities of particular interest to cosmology are the anticipated present day coherence length and magnetic field strength given particular initial conditions immediately after the epoch of magnetogenesis. We have shown that whereas strong magnetic fields $B \gg B_c^{\eta} \approx 10^{-13}$ G are essentially undergoing no further evolution (i.e., growth of $L^{>}$) after recombination weak fields $B \lesssim B_C^{\eta}$ do. In either case, after the later epoch of reionization the distinction between strong and weak disappears such that any reasonable strength field is turbulent at present. The present day field strengths are then simply obtained by applying Eq. (79) with $v \approx v_{\rm A}$ today. This yields the correlation

$$B_0 \approx 5 \times 10^{-12}\ \mathrm{G}\left(\frac{L_c}{\mathrm{kpc}}\right) \tag{80}$$

between magnetic field strength and magnetic correlation length [52]. The magnetic correlation length itself is given by the initial conditions after the epoch of magnetogenesis [cf. Eqs. (69) and (74) for the submaximal helical and maximally helical cases, respectively, with example values for an $n = 3$ spectrum given in Eqs. (71)–(73) and for fields which during the course of evolution have become maximally helical in Eqs. (76)–(78)]. Both quantities are shown for nonhelical fields as a function of spectral index and magnetogenesis temperature in Figs. 16 and 17.

Concerning the evolution of maximally helical fields we have found and reverified prior work [17] on the intriguing property of self-similar evolution of such fields. In particular, though maximal helical fields keep their initial spectral index on large scales (i.e., for $L \gtrsim L^{>}$) the amplitude of the large-scale tail of magnetic fluctuations is subject to a seemingly ''acausual'' amplification on scales which are far larger than the distance an Alfvén wave may travel (cf. Figs. 6 and 10). The large-scale magnetic field spectrum for maximally helical fields is given by Eq. (46), whereas Eq. (44) describes that of submaximally helical fields. We have numerically disputed the claimed effect (e.g.,[20,21]) that maximally helical fields do not excite fluid motions and are therefore not subject to viscous damping (cf. Sec. II B). Rather, only due to the excitation of fluid motions the magnetic correlation length of maximally helical fields may continuously grow during the evolution of the early Universe. It is important to note that due to the large dynamic increase

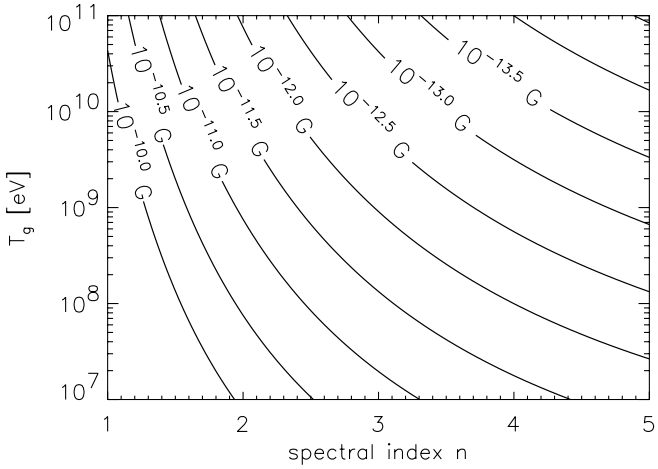

FIG. 16. Shown is the final magnetic field strength, $B(T_0)$, for submaximal (i.e., $L < L^{\max}$) magnetic fields in the (n, T_g) parameter space. Here, the initial magnetic field strength is $r_g = 0.01$. Results for different r_g may be obtained by scaling the field strength by $(r_g/0.01)^{1/2}$.

of $L^{>}$ between the epoch of magnetogenesis and the present (and the associated large dissipation of magnetic energy) a field with a minute amount of initial helicity typically evolves into a maximally helical field at present. This happens when the magnetic correlation length has grown beyond that given in Eq. (45). Figure 18 shows the amount of initial helicity, h_g [cf. Eq. (38)] as a function of magnetic spectral index required to reach a maximally helical state at present. Completely helical fields may thus not necessarily be considered an unlikely remnant of the early Universe. The current magnetic field strength and correlation length of magnetic fields which became maxi-

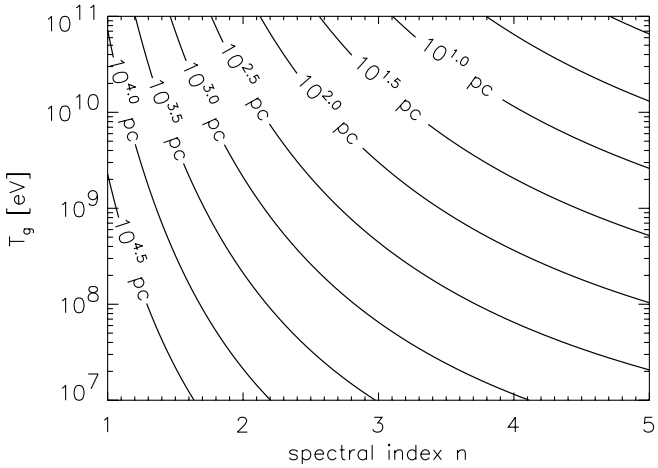

FIG. 17. Shown is the final coherence length, $L(T_0)$, of submaximal magnetic fields (i.e., $L < L^{\max}$) in the (n, T_g) parameter space. Here, the initial magnetic field strength is $r_g = 0.01$. Results for different r_g may be obtained by scaling the coherence length by $(r_g/0.01)^{1/2}$.

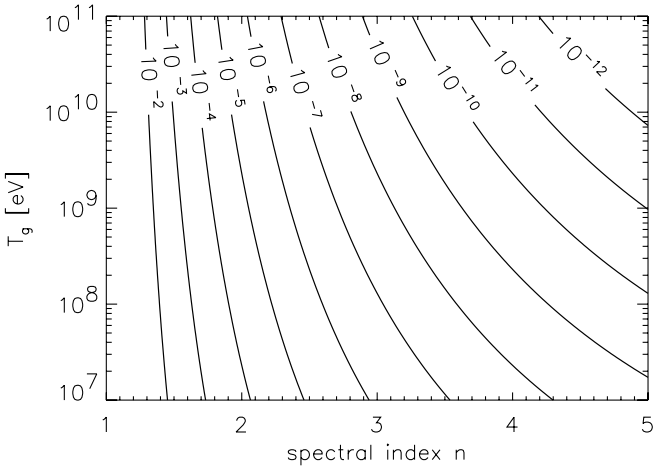

FIG. 18. Shown is the minimal relative initial magnetic helicity, h_g, necessary for a magnetic field to have become maximal helical (i.e., $L \gtrsim L^{\max}$) at the present epoch. For instance, initial magnetic fields generated at $T_g = 100$ MeV with $n = 3$ become maximal helical if $h_g \gtrsim 1.2 \times 10^{-7}$. Note, this condition is independent of the initial magnetic field strength, r_g.

mal helical are shown in Figs. 19 and 20 as a function of initial helicity and magnetogenesis temperature.

The evolution of magnetic fields during epochs with intermediate redshifts $z \approx 10^3$–10^7 is described by turbulent evolution at higher redshifts, followed by a viscous MHD period without further growth of $L^{>}$, and a viscous MHD period with comparatively rapid growth of $L^{>}$ with viscosity due to free-streaming photons (cf. Figs. 12 and 14). For essentially all interesting magnetic field strengths and spectra the plasma is, in this last state shortly before recombination, allowing for the prediction of a correlation

$$B_{\rm rec} \approx 8 \times 10^{-11}\ {\rm G}\left(\frac{L_c}{\rm kpc}\right) \tag{81}$$

between magnetic field strength and correlation length shortly before recombination. Equation (81) is obtained via Eq. (79) and noting that $v \approx v_{\rm A}^2/(\alpha_\gamma L)$ during viscous photon free streaming. The correlation length to be employed in Eq. (81) may be derived only when the initial conditions shortly after the magnetogenesis scenario are known, i.e., via Eq. (62) and the comments further below concerning maximally helical fields, whereas the instantaneous spectra are again given by Eqs. (44) and (46).

The correlation in Eq. (81) is almost identical to what one expects from a linear analysis (JKO98). In contrast, for the formulation of limits on primordial magnetic fields due to magnetic field dissipation at redshift $z \approx 2.5 \times 10^6$ and the concomitant production of spectral μ distortions in the CMBR, Ref. [26] has employed the results of a linear analysis leading to the claim that fields of 3×10^{-8} G on scales of 400 pc are disallowed. Though the limiting field strength does not change when nonlinear evolution is considered, as it is an energetic constraint, the comoving length scale does. This is due to the bulk of energy not being contained on the dissipation scale (at ~400 pc) but rather on the integral scale given by applying Eq. (80) at $z \approx 2.5 \times 10^6$. However, coincidentally the change is only mild, moving the limiting scale from 400 pc up to 1 kpc, since for such field strength the flow at $z \approx 2.5 \times 10^6$ is only mildly turbulent (i.e., $R_e \approx 100$) and since in the viscous regime both treatments almost coincide. When $B \gtrsim B_c^\eta$ the cosmic recombination process is associated with an almost instantaneous jump in the magnetic correlation length. How large this jump is then depends on the magnetic field

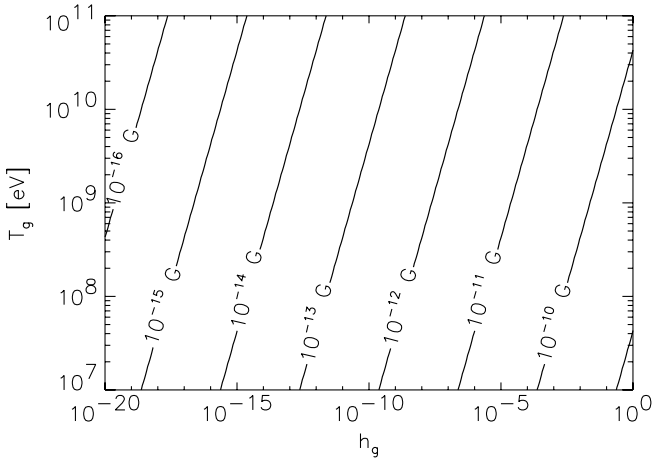

FIG. 19. Shown is the final magnetic field strength, $B(T_0)$, for magnetic fields which have become maximal helical (i.e., $L \gtrsim L^{\max}$) in the (h_g, T_g) parameter space. Here, the initial magnetic field strength is $r_g = 0.01$, and for different r_g the results scale with $(r_g/0.01)^{1/2}$. Note the absence of a dependence on spectral index n.

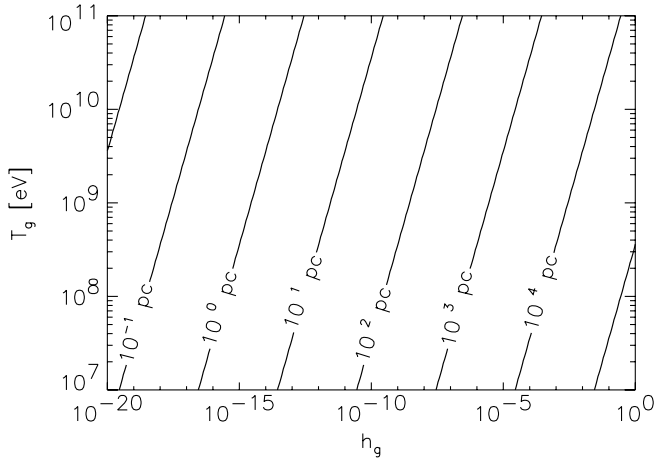

FIG. 20. Shown is the final coherence length, $L(T_0)$, for magnetic fields which became maximal helical (i.e., $L \gtrsim L^{\max}$) in the (h_g, T_g) parameter space. Here, the initial magnetic field strength is $r_g = 0.01$, and for different r_g results may be rescaled by $(r_g/0.01)^{1/2}$.

spectral index determined during the magnetogenesis epoch. It would be interesting to examine at what field strength the associated energy dissipation could impact on the recombination process itself, especially in light of fields with strength $B \gtrsim 6 \times 10^{-11}$ G being able to produce small-scale density perturbations as then $v_A \gtrsim v_b$ [cf. Eqs. (33)–(35)].

With the advances in high-precision CMBR anisotropy observations the interest in putative signals due to primordial magnetic fields has immensely risen. Essentially all current magnetic field induced CMBR anisotropy examinations assume fields of strengths $\sim 10^{-10}$–10^{-9} G on scales roughly the Silk scale, $L \approx 10$ Mpc. This is done, of course, since for much weaker fields the signal is hardly observable and when moving to much smaller scales not only are satellite missions like the Wilkinson Microwave Anisotropy Probe and Planck not able to resolve these but also the signals are naively expected to be reduced due to the thickness of the last scattering surface $\sigma \approx 10$ Mpc. By inspection of Eq. (81) it is clear that the scale of ~ 10 Mpc may not be the integral scale but rather a scale much beyond. We argue here that unless substantial primordial magnetic fields have their origin during an inflationary phase a search for primordial magnetic fields of $\sim 10^{-9}$ G on 10 Mpc seems futile (at best controversial). This is due to a number of reasons. First, with fields which are causally generated during, for example, early cosmic phase transitions such strengths on these scales are impossible to reach. This is of course due to the smallness of the Hubble scale in the very early Universe and since due to causality the spectrum must be sufficiently blue. Second, due to the blueness of the spectrum of causally generated magnetic fields, limits on smaller scales are easily violated. Figure 21 shows the maximum possible magnetic field strength on the scale 10 Mpc as a function of magnetic field spectral index. Fields which are above this value produce CMBR spectral μ distortions in excess of those observed [26]. It is seen that only for unrealistically small spectral indices $B \sim 10^{-9}$ G on 10 Mpc may be reached. Finally, a direct constraint on the scale ~ 10 Mpc may be applied when the low-redshift collapse of a magnetized plasma to a cluster is considered [53]. It is found that pre-cluster-collapse fields of 4×10^{-12} G (corresponding to the authors 10^{-9} G at redshift $z = 15$) are sufficient to reproduce observed Faraday rotation measures in present day clusters. Larger fields seem to overproduce the Faraday rotation measure and should therefore be ruled out.

When trying to detect primordial magnetic fields a more promising and realistic alley should be the search for CMBR anisotropies on very small scales, in particular, on scales ~ 10 kpc (corresponding to multipoles $l \sim 10^6$), possibly close or only slightly above the integral scale, rather than the canonical 10 Mpc (multipoles $l \sim 10^3$). This is due to the existence of viable scenarios

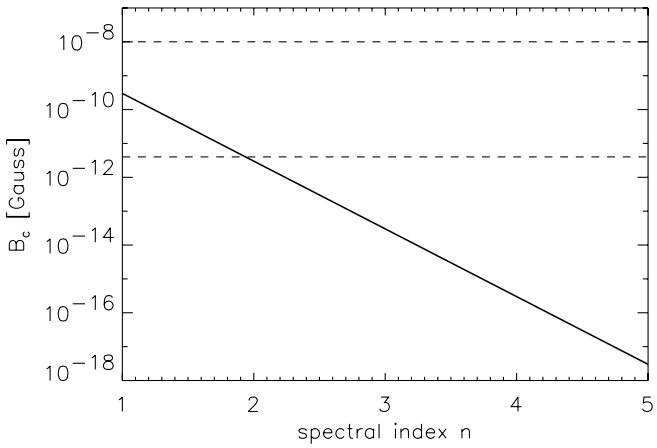

FIG. 21. Exclusion plot on the comoving magnetic field strength on $L = 10$ Mpc (equally applicable to the present epoch and recombination) as a function of magnetic field spectral index. The solid line shows the upper limit on $B_c(10\ \mathrm{Mpc})$ from an excessive distortion of the CMBR blackbody spectrum by magnetic field dissipation at redshift $z = 3 \times 10^6$ [26], whereas the horizontal lines (from top to bottom) show the upper limits from present day intergalactic Faraday rotation measurements [2] and the possible overproduction of cluster-magnetic fields (see text), respectively.

producing fields of interesting amplitude $\sim 10^{-9}$ G on such scales and further such fields evading constraints from CMBR spectral distortions and observed cluster-magnetic fields. Moreover, though this scale is much below the width of the last scattering surface, the expected signal is not necessarily small. In particular, for small scales $l \lesssim 1$ Mpc the magnetic field induced peculiar velocities are $v \approx v_A^2/(\alpha_\gamma l)$. CMBR temperature fluctuations follow $\delta T/T \propto v$ and for scales $l < \sigma$ are additionally suppressed by $\sqrt{l/\sigma}$ due to the thickness of the last scattering surface. Combing these factors one finds $\delta T/T \propto l^{-n-1/2}$ for $l \gtrsim L$, thus an increasing signal with decreasing scale. Here n is the spectral index of the primordial magnetic field. Primordial magnetic fields should therefore leave their strongest CMBR signal on small scales $l \sim 10^6$. It remains to be seen if contamination of the primordial CMBR anisotropies by foregrounds may pose serious problems to such observations.

Last but not least, we have already challenged in a prior publication [54] the long-standing and widespread belief that cluster-magnetic fields may not be entirely of primordial origin. It is typically argued that causal magnetogenesis scenarios (as, for example, due to local processes during the QCD or electroweak transitions) yield only weak magnetic fields $\lesssim 10^{-20}$ G on the (precollapse) scale of a cluster of galaxies. Since during cluster collapse further magnetic field amplification by only modest factors 10^3–10^5 due to magnetic flux conservation result, starting from 10^{-20} G implies that one is still far from the observed μG fields in clusters, requiring further field

amplification processes such as a dynamo. The problem with this argument is that, *a priori*, it is not clear if the initial magnetic fields have to reside on the cluster scale itself, or if magnetic field energy density contained on much smaller scales may during the collapse be transferred to the cluster scale. In fact, the only numerical simulation of the collapse of a magnetized plasma to a cluster to date [53] seems to indicate an approximate independence of the final result on initial magnetic coherence length, with the final cluster Faraday rotation measures only dependent on the precollapse magnetic-energy density (required are $B \approx 4 \times 10^{-12}$ G). It is currently not clear by what mechanism magnetic energy may inverse cascade from small scales to large scales during the cluster collapse. But if indeed it does, cluster-magnetic fields could be entirely primordial, since magnetic fields of $\sim 10^{-12}$–10^{-11} G on approximately $\sim$kpc scales are possible by either having magnetogenesis occur late, during the QCD phase transition, and/or magnetogenesis scenarios which generate a very small amount of initial helicity [cf. Eqs. (69), (74), and (80)]. It is interesting to note that such a scenario also led to a "prediction" of magnetic field strength and amplitudes in voids, far from galaxies. Fields in such environments are presumably not affected by magnetic fields in galactic outflows and could be in the optimistic case observable by future technology [8–10].

ACKNOWLEDGMENTS

We acknowledge technical assistance and emotional support by T. Abel, A. Kercek, and M. Mac Low in undertaking this study.

APPENDIX A: THE MHD EQUATIONS IN MINKOWSKI SPACE

We are using Gaussian natural units, i.e., $\mu_0 = 1 = \epsilon_0$, and $c = 1$, for solving the MHD equations. On a static background in the Newtonian and nonrelativistic limit the MHD equations are given by (see, e.g., [55])

$$\frac{\partial \varrho}{\partial t} + \nabla \cdot (\mathbf{v}\varrho) = 0, \tag{A1}$$

$$\frac{\partial \mathbf{v}}{\partial t} + (\mathbf{v} \cdot \nabla)\mathbf{v} = -\frac{1}{\varrho}\nabla p - \frac{\mathbf{B} \times (\nabla \times \mathbf{B})}{4\pi\varrho} - \nabla\Phi, \tag{A2}$$

$$\frac{\partial \mathbf{B}}{\partial t} = \nabla \times (\mathbf{v} \times \mathbf{B}) + \frac{1}{4\pi\sigma}\nabla^2\mathbf{B}, \tag{A3}$$

$$\triangle\Phi = 4\pi\varrho, \tag{A4}$$

where ϱ, $\mathbf{v}$, p, $\mathbf{B}$, Φ, and σ are matter density, fluid velocity, thermal pressure, magnetic field, gravitational potential, and electrical conductivity, respectively. The above equations have to be closed by an equation of state.

APPENDIX B: CONFORMAL PROPERTIES OF THE MHD EQUATIONS IN AN EXPANDING UNIVERSE

In the following we assemble the MHD equations in the FRW universe with the scale factor a and the Hubble parameter H for (a) relativistic MHD, i.e., when photons are still coupled to the plasma on the scale of the magnetic fluctuations, $l_\gamma \ll L$, and (b) for nonrelativistic MHD in the opposite limit $l_\gamma \gg L$. In both limits, the equation of state in the early Universe is well approximated by being isothermal due to incompressibility in the limit (a) and due to the efficiency of electron-photon Thomson scattering and the associated cooling in the limit (b). We then show how in both limits the MHD equations in the FRW background may be essentially reduced to those in Minkowski space, when appropriate scalings with a scale factor of the physical quantities are introduced. For further details on the derivation of the equations we refer the reader to JKO98. To lowest nontrivial order in $1/\sigma$, the relativistic MHD equations are

$$\frac{\partial \varrho}{\partial t} + \frac{1}{a}\nabla \cdot ((\varrho + p)\mathbf{v}) + 3H(\varrho + p) = 0, \tag{B1}$$

$$\left[\frac{\partial}{\partial t} + \frac{1}{a}(\mathbf{v} \cdot \nabla) + H\right]\mathbf{v} + \frac{\mathbf{v}}{\varrho + p}\frac{\partial p}{\partial t} + \frac{1}{a}\frac{\nabla p}{\varrho + p} + \frac{1}{a}\left(\frac{\mathbf{B} \times (\nabla \times \mathbf{B})}{4\pi(\varrho + p)}\right) = \frac{\eta}{a^2}\left[\nabla^2\mathbf{v} + \frac{1}{3}\nabla(\nabla \cdot \mathbf{v})\right], \tag{B2}$$

$$\left(\frac{\partial}{\partial t} + 2H\right)\mathbf{B} = \frac{1}{a}\nabla \times (\mathbf{v} \times \mathbf{B}) + \frac{1}{4\pi\sigma a^2}\nabla^2\mathbf{B}, \tag{B3}$$

where we assumed that $\varrho_{\rm em} \ll \varrho = \varrho_{\rm fluid}$ (here ϱ refers to internal energy density for radiation) and we kept only terms of the lowest order in v/c. The shear viscosity η is given by [56]

$$\eta = \frac{4}{15}\frac{\pi^2}{30} g_t T^4 l_{\rm mfp}/(\varrho + p), \tag{B4}$$

where g_t is the number of relativistic degrees of freedom of the particles with the longest mean free path $l_{\rm mfp}$. Using the following the rescaled variables (e.g., [14,16,57]):

$$\begin{aligned} &\tilde{\varrho} \equiv \varrho a^4, \qquad \tilde{p} \equiv p a^4, \qquad \tilde{\mathbf{B}} \equiv \mathbf{B} a^2, \\ &\tilde{\mathbf{v}} \equiv \mathbf{v}, \qquad \tilde{T} \equiv T a, \qquad \tilde{\eta} \equiv \eta a^{-1}, \\ &d\tilde{t} \equiv dt a^{-1}, \qquad \tilde{\sigma} \equiv \sigma a, \end{aligned} \tag{B5}$$

the MHD Eqs. (B1)–(B3) in the radiation dominated universe (i.e., $a \propto t^{-1/2}$ and $p = \varrho/3$) can be written as

$$\frac{\partial \tilde{\varrho}}{\partial \tilde{t}} + \nabla \cdot ((\tilde{\varrho} + \tilde{p})\tilde{\mathbf{v}}) = 0, \tag{B6}$$

$$\left[\frac{\partial}{\partial\tilde{t}}+(\tilde{\mathbf{v}}\cdot\nabla)\right]\tilde{\mathbf{v}}+\frac{\tilde{\mathbf{v}}}{\tilde{\varrho}+\tilde{p}}\frac{\partial\tilde{p}}{\partial\tilde{t}}+\frac{\nabla\tilde{p}}{\tilde{\varrho}+\tilde{p}}+\frac{\tilde{\mathbf{B}}\times(\nabla\times\tilde{\mathbf{B}})}{4\pi(\tilde{\varrho}+\tilde{p})}$$
$$=\tilde{\eta}\left[\nabla^2\tilde{\mathbf{v}}+\frac{1}{3}\nabla(\nabla\cdot\tilde{\mathbf{v}})\right], \tag{B7}$$

$$\frac{\partial\tilde{\mathbf{B}}}{\partial\tilde{t}}=\nabla\times(\tilde{\mathbf{v}}\times\tilde{\mathbf{B}})+\frac{1}{4\pi\sigma}\nabla^2\tilde{\mathbf{B}}. \tag{B8}$$

A similar rescaling transformation can be done in the MD regime (i.e., $a\propto t^{3/2}$ and $p\ll\varrho$) using *super comoving variables* [58]:

$$\tilde{\varrho}\equiv\varrho a^3,\qquad \tilde{p}\equiv pa^4,\qquad \tilde{\mathbf{B}}\equiv\mathbf{B}a^2,$$
$$\tilde{\mathbf{v}}\equiv\mathbf{v}a^{1/2},\qquad \tilde{\eta}\equiv\eta a^{-1/2},\qquad d\tilde{t}\equiv dta^{-3/2}, \tag{B9}$$
$$\tilde{H}\equiv a^{3/2}H,\qquad \tilde{\sigma}\equiv\sigma a^{1/2}.$$

The transformations yield almost the form of the ordinary nonrelativistic MHD equations [cf. Eqs. (A1)–(A3)]:

$$\frac{\partial\tilde{\varrho}}{\partial\tilde{t}}+\nabla\cdot(\tilde{\varrho}\,\tilde{\mathbf{v}})=0, \tag{B10}$$

$$\frac{\partial\tilde{\mathbf{v}}}{\partial\tilde{t}}+(\tilde{\mathbf{v}}\cdot\nabla)\tilde{\mathbf{v}}+\frac{1}{\tilde{\varrho}}\nabla\tilde{p}+\frac{1}{4\pi\tilde{\varrho}}\tilde{\mathbf{B}}\times(\nabla\times\tilde{\mathbf{B}})=-\tilde{\mathbf{s}}, \tag{B11}$$

$$\frac{\partial\tilde{\mathbf{B}}}{\partial\tilde{t}}-\nabla\times(\tilde{\mathbf{v}}\times\tilde{\mathbf{B}})=\frac{1}{4\pi\sigma}\nabla^2\tilde{\mathbf{B}}. \tag{B12}$$

Here, the dissipation term is

$$\tilde{\mathbf{s}}=\frac{1}{2}\tilde{H}\,\tilde{\mathbf{v}}-\tilde{\eta}\left[\nabla^2\tilde{\mathbf{v}}+\frac{1}{3}\nabla(\nabla\cdot\tilde{\mathbf{v}})\right], \tag{B13}$$

where ϱ is again matter density. Here the term $\frac{1}{2}\tilde{H}\,\tilde{\mathbf{v}}$ in Eq. (B13) represents the only difference to the MHD equations in Minkowski space and may be interpreted as a drag term. In particular, fluid momentum dissipation due to a homogeneous photon background with $l_\gamma\gg L$, i.e., photon drag, is described by the addition of a term $-\alpha\mathbf{v}$ on the RHS of Eq. (B2) due to free-streaming photons (and the dropping of the terms proportional to shear viscosity η due to diffusing photons). In the scaled variables this leads to the following dissipation term:

$$\tilde{\mathbf{s}}=(\tfrac{1}{2}\tilde{H}+\tilde{\alpha})\tilde{\mathbf{v}} \tag{B14}$$

with $\tilde{\alpha}=a^{3/2}\alpha$.

APPENDIX C: DISSIPATION OF ENERGY AND HELICITY

With a homogeneous density and pressure distribution the total energy density is given by

$$E=\frac{\varrho+p}{2}\frac{1}{V}\int_V d^3x(\mathbf{v}^2+\mathbf{v}_{\rm A}^2), \tag{C1}$$

where $\mathbf{v}_{\rm A}=\mathbf{B}/\sqrt{4\pi(\varrho+p)}$ is the Alfvén velocity. The magnetic helicity density is

$$\mathcal{H}\equiv\frac{1}{V}\int_V d^3x\mathbf{A}\cdot\mathbf{B}, \tag{C2}$$

where $\mathbf{A}$ is the vector potential, i.e., $\mathbf{B}=\nabla\times\mathbf{A}$. Using the MHD equations of Appendix A the time evolution of the above quantities is given by (up to surface terms)

$$V\frac{dE}{dt}=-\eta(\varrho+p)\int_V d^3x(\nabla\times\mathbf{v})^2$$
$$-\frac{1}{(4\pi)^2\sigma}\int_V d^3x(\nabla\times\mathbf{B})^2, \tag{C3}$$

$$V\frac{d\mathcal{H}}{dt}=-\frac{1}{2\pi\sigma}\int_V d^3x\mathbf{B}\cdot(\nabla\times\mathbf{B}). \tag{C4}$$

In the case when fluid momentum dissipation occurs by free-streaming particles rather than diffusing particles, i.e., $\eta\nabla^2\mathbf{v}\to-\alpha\mathbf{v}$, the first integrand (and prefactor) of the RHS of Eq. (C3) must be replaced by $\alpha\varrho\mathbf{v}^2$. Note that in the case of *ideal* MHD (i.e., $\sigma\to\infty$) the helicity (C2) becomes a conserved quantity. In Fig. 22 we present the results of our resolution study for helicity conservation which show increasingly conserved magnetic helicity with increasing resolution. Simulations with $\geq 128^3$ grid points do not exhibit significant loss of magnetic helicity over several dynamical times.

In the radiation dominated regime the shear viscosity is given by (cf. also JKO98)

$$\eta=\frac{1}{5}\frac{g_t}{g_f}l_{\rm mfp}, \tag{C5}$$

with $l_{\rm mfp}$ being the mean free path of neutrinos or photons with statistical weight g_t, and where g_f denotes the

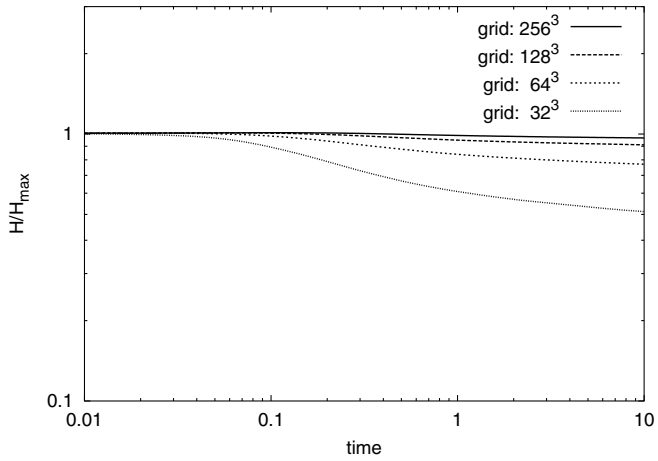

FIG. 22. Time evolution of the magnetic helicity $\mathcal{H}$ in the case of a maximal helical magnetic field. The loss of helicity is due to magnetic diffusion, which is solely due to numerical diffusion which can be seen by the resolution study.

statistical weight of the total fluid energy radiation density. Here, the photon mean free path, $l^{\gamma}_{\rm mfp} = 1/(\sigma_{\rm T} n_e)$, as measured in comoving units, is

$$l^{\gamma}_{{\rm mfp},c} \approx 1.77\ {\rm Mpc} X_e^{-1} \left(\frac{\Omega_b h^2}{0.02}\right)^{-1} \left(\frac{T}{0.26{\rm eV}}\right)^{-2}, \quad \text{(C6)}$$

for $T \lesssim 20\,{\rm keV}$. For the neutrino mean free path we assume $l^{\nu}_{\rm mfp} \simeq 1/[G_F^2 T^2 (n_l + n_q)]$ (with the Fermi constant $G_F \approx 1.1663 \times 10^{-5}\ {\rm GeV}^{-2}$ and the number densities n_l and n_q of relativistic leptons and quarks, respectively). We find at $T = 2.6\,{\rm MeV}$ the comoving value

$$l^{\nu}_{{\rm mfp},c} \simeq 6.7\ {\rm pc} \left(\frac{g_l + g_q}{8.75}\right)^{-1} \left(\frac{T}{2.6\ {\rm MeV}}\right)^{-4}, \quad \text{(C7)}$$

where $g_l = (7/8)10$ and $g_q = 0$ has been assumed. Note that when using Eq. (C7) for the computation of α_ν care has to be taken to not only include scattering but also neutrino annihilation (cf. [59]). On the other hand, neutrino self-scattering does not contribute such that, below the QCD transition, g_l should be effectively reduced to 3.5 (only $e^{\pm}$). We use the following drag coefficients for neutrinos and photons, respectively [59,60]

$$\alpha_\nu \simeq \frac{g_\nu}{g_f} \frac{1}{l^{\nu}_{\rm mfp}}, \quad \text{(C8)}$$

$$\alpha_\gamma \simeq \frac{4}{3} \frac{\varrho_\gamma}{\varrho_b} \frac{1}{l^{\gamma}_{\rm mfp}} \approx \frac{4}{3} X_e \frac{\sigma_{\rm T} \varrho_\gamma}{m_p}, \quad \text{(C9)}$$

with $\sigma_{\rm T}$ the Thomson cross section, m_p the proton mass, and ϱ_γ, ϱ_b denoting photon and baryon densities, respectively. In the high temperature regime ($1\,{\rm MeV} \lesssim T \lesssim m_W$) the electrical conductivity σ is given by [61]

$$0.76T \lesssim \sigma \lesssim 6.7T, \quad \text{(C10)}$$

where the larger value refers to the upper temperature bound. At temperatures below the electron mass the conductivity becomes [55]

$$\sigma = \frac{\alpha n_e \tau_c}{m_e} \simeq \frac{m_e}{\alpha \ln\Lambda} \left(\frac{2}{\pi} \frac{T}{m_e}\right)^{3/2}, \quad \text{(C11)}$$

where τ_c is the mean time between two collisions, $\Lambda = (1/6\pi^{1/2})(1/\alpha^{1/2})(m_e^3/n_e)^{1/2}(T/m_e)$, and α, m_e, and n_e are fine structure constant, electron mass, and electron density, respectively. The magnetic Prandtl number P_m which gives the relative importance of the kinetic and magnetic diffusion is very large in the early Universe,

$$P_m = 4\pi\eta\sigma \simeq 2.9 \times 10^8 \left(\frac{\rm keV}{T}\right)^{3/2} \quad \text{(C12)}$$

for $T < m_e$. This allows one to neglect the dissipation of magnetic field energy due to finite conductivity. We use the ion-neutral momentum transfer at low temperatures given by [62]

$$\alpha_{\rm in} \approx 3.2 \times 10^{-9}\ {\rm s}^{-1} \left(\frac{n_H}{\rm cm^{-3}}\right) = \alpha_{\rm in} \Omega_b h^2 \left(\frac{a}{a_0}\right)^{-3}, \quad \text{(C13)}$$

where $\alpha_{\rm in} \equiv 4.4 \times 10^{-14}\ {\rm s}^{-1}$ (note $\alpha_{\rm in} \neq \alpha_{\rm ni}$), $n_H \approx n_b$ denotes hydrogen density, and a_0 is the present day scale factor. The hydrogen mean free path $l^{H}_{\rm mfp}$ after recombination is determined by hydrogen-hydrogen elastic scattering. Scattering on electrons (or protons) may be neglected in computing $l^{H}_{\rm mfp}$ due to the small degree of ionization (i.e., $X_e \approx 4 \times 10^{-4}$). Assuming a temperature independent [63], cross section which is approximately $\sigma_{HH} \approx \pi a_{\rm B}^2$, where $a_{\rm B} = 5.29 \times 10^{-9}\,{\rm cm}$ is the Bohr radius one finds

$$l^{H}_{{\rm mfp},c} \approx 9.9 \times 10^{-3}\ {\rm pc} \left(\frac{\sigma_{HH}}{10^{-16}\ {\rm cm}^2}\right)^{-1} \left(\frac{T}{0.259\ {\rm eV}}\right)^{-2} \quad \text{(C14)}$$

for the comoving mean free path. Shear viscosity due to hydrogen-hydrogen elastic scattering may be estimated by

$$\eta_{HH} \sim \frac{1}{3} v^{\rm th}_H l^{H}_{\rm mfp} \approx 8.0 \times 10^{18} \frac{\rm cm^2}{\rm s} \left(\frac{\sigma_{HH}}{10^{-16}\ {\rm cm}^2}\right)^{-1} \times \left(\frac{T}{0.259\ {\rm eV}}\right)^{-5/2}, \quad \text{(C15)}$$

where $v^{\rm th}_H = \sqrt{3T/m_p}$ denotes hydrogen thermal velocity. Finally we estimate the mean free path of electrons in the plasma. After recombination, and with an effective cross section $\sigma \sim (\alpha/T_e)^2$ [64], where α is the fine structure constant and T_e the electron temperature we find

$$l^{e}_{{\rm mfp},c} \sim 10^{-2}\ {\rm pc} \quad \text{(C16)}$$

between the epochs with redshift $z \approx 1100$ and $z \approx 100$. Note that the comoving mean free path is independent of temperature. Below redshift $z \approx 100$ the mean free path decreases even further due to a more rapid decrease in electron temperature than photon temperature. We take a constant ionization fraction after recombination of

$$X_e \approx 4 \times 10^{-4} \quad \text{(C17)}$$

neglecting residual dependencies on Ω_b and Ω.

APPENDIX D: GENERATION OF HELICAL FIELDS

To excite a stochastic magnetic field with or without initial helicity we choose a coordinate system in k space useful for helical fields with the orthogonal unit vectors $\{\mathbf{e}_+, \mathbf{e}_-, \hat{\mathbf{k}}\}$ (see, e.g., [55]). By expanding the Fourier transformed vector potential $\hat{\mathbf{A}}$ in this basis, i.e.,

$$\hat{\mathbf{A}}_{\mathbf{k}} = A^{+}_{\mathbf{k}} \mathbf{e}_+ + A^{-}_{\mathbf{k}} \mathbf{e}_- + A^{k}_{\mathbf{k}} \hat{\mathbf{k}}, \quad \text{(D1)}$$

one obtains the magnetic field in the new basis

$$\hat{\mathbf{B}}_{\mathbf{k}} = -i\mathbf{k} \times \hat{\mathbf{A}}_{\mathbf{k}} = -k(A^+_{\mathbf{k}}\mathbf{e}_+ - A^-_{\mathbf{k}}\mathbf{e}_-). \quad \text{(D2)}$$

With this set of basis vectors the magnetic field spectra are given by (cf. also [17])

$$|\hat{\mathbf{B}}_{\mathbf{k}}|^2 = k^2(|A^+_{\mathbf{k}}|^2 + |A^-_{\mathbf{k}}|^2), \quad \text{(D3)}$$

whereas the magnetic helicity becomes

$$\mathcal{H} = \frac{1}{(2\pi)^3}\int d^3k \hat{\mathbf{A}}^*_{\mathbf{k}} \cdot \hat{\mathbf{B}}_{\mathbf{k}} = \frac{1}{(2\pi)^3}\int d^3k H_{\mathbf{k}} \quad \text{(D4)}$$

with

$$H_{\mathbf{k}} \equiv \hat{\mathbf{A}}^*_{\mathbf{k}} \cdot \hat{\mathbf{B}}_{\mathbf{k}} = -k(|A^+_{\mathbf{k}}|^2 - |A^-_{\mathbf{k}}|^2). \quad \text{(D5)}$$

Note that this choice of coordinate system reflects also that the helicity (D4) is a well-defined physical quantity as it is gauge independent, i.e., independent of $A^k_{\mathbf{k}}$. To ensure a real vector potential $\mathbf{A}(\mathbf{x})$ and from that a real magnetic field $\mathbf{B}(\mathbf{x})$ the $A^{\pm}_{\mathbf{k}}$ have to fulfill the relation

$$(A^{\pm}_{\mathbf{k}})^* = -A^{\pm}_{-\mathbf{k}}. \quad \text{(D6)}$$

The magnetic helicity can be of either sign but the magnitude $|H_{\mathbf{k}}|$ is limited by the relation

$$|H_{\mathbf{k}}| \leq k^{-1}|\hat{\mathbf{B}}_{\mathbf{k}}|^2. \quad \text{(D7)}$$

A magnetic field is said to be maximally helical if the equals sign in the above equation holds. From the relations (D3) and (D5) it can be seen that the strength of the magnetic field can be chosen independently of the magnetic helicity [in this approach one can consider either $(A^+_{\mathbf{k}}, A^-_{\mathbf{k}})$ or $(B_{\mathbf{k}}, H_{\mathbf{k}})$ as independent variables]. This allows one to excite stochastic magnetic fields with arbitrary helicity. To excite stochastic magnetic fields with a fractional helicity we choose

$$A^-_{\mathbf{k}} \equiv \sqrt{f}A^+_{\mathbf{k}}, \quad \text{(D8)}$$

where $f \in [0, 1]$. This convention leads to

$$|H_{\mathbf{k}}| = \frac{1}{k}|\hat{\mathbf{B}}_{\mathbf{k}}|^2\frac{1-f}{1+f} \quad \text{(D9)}$$

for the magnitude of the helicity in terms of the magnetic field. From Eq. (D9) it can be seen that $(1 - f)/(1 + f)$ is the fraction of the maximal helicity magnitude $H_{\max} = k^{-1}|\hat{\mathbf{B}}_{\mathbf{k}}|^2$. This can be used to adjust the magnetic helicity to an arbitrary magnitude.

Note that the choice of exciting magnetic fields with a fractional helicity (D9) is not unique. This particular choice just reduces the amplitude of the helicity spectra (compared to that of the maximal helicity spectra) by a factor of $(1 - f)/(1 + f)$. For nonmaximal helicity it is also possible that the helicity spectra $H_{\mathbf{k}}$ do not follow the spectra of the magnetic field $|\hat{\mathbf{B}}_{\mathbf{k}}|^2$, but are rather independently distributed in k space. The particular choice of the implementation of a fractional helicity may influence the evolution of magnetic fields.

APPENDIX E: NUMERICAL METHODS

We performed the numerical simulation using ZEUS-3D [27,28,65]. All simulations were performed with periodic boundary conditions. This mimics an infinitely large volume, where the surface integrals of the MHD variables around the entire box vanish exactly. Furthermore, we extended the code for the purposes of our studies. We used a Gaussian random field for the initial fluctuations of the magnetic components with *zero mean*. To ensure a divergence-free magnetic field this is done by exciting modes of the vector potential $\hat{\mathbf{A}}_{\mathbf{k}}$ in k space in the following way: The complex vector potential $\hat{\mathbf{A}}_{\mathbf{k}} = (\hat{A}^1_{\mathbf{k}}, \hat{A}^2_{\mathbf{k}}, \hat{A}^3_{\mathbf{k}})$ is generated by

$$\hat{A}^i_{\mathbf{k}} = |\hat{A}^i_{\mathbf{k}}|e^{i\varphi_{\mathbf{k}}} \qquad i \in [1, 2, 3], \quad \text{(E1)}$$

where the amplitudes $|\hat{A}^i|$ are randomly selected using a Gaussian distribution, i.e.,

$$P(|\hat{A}^i_{\mathbf{k}}|) = \frac{1}{\sqrt{2\pi}\sigma_{\mathbf{k}}}\exp\left\{-\frac{|\hat{A}^i_{\mathbf{k}}|^2}{2\sigma^2_{\mathbf{k}}}\right\}, \quad \text{(E2)}$$

and the phases $\varphi_{\mathbf{k}}$ are randomly selected with a uniform distribution from the interval $[0, 2\pi]$. The amplitudes are related to the variance $\sigma_{\mathbf{k}}$ by

$$|\hat{A}^i_k|^2 \propto \sigma^2_k \propto k^n, \quad \text{(E3)}$$

where we assumed an isotropic universe, i.e., $\hat{A}^i_{\mathbf{k}} = \hat{A}^i_k$. These modes were excited up to a cutoff k_c. The initial stochastic velocity field is generated in the same way as the initial magnetic field described above. In addition one can either generate the stochastic velocity field $\mathbf{v}$ by using Eq. (E2) directly, or one can generate a *divergence-free* velocity field by first exciting a vector potential $\mathbf{A}$ and then computing $\mathbf{v} = \nabla \times \mathbf{A}$. The latter avoids strong density perturbations.

[1] R. Beck, A. Brandenburg, D. Moss, A. Shukurov, and D. Sokoloff, Annu. Rev. Astron. Astrophys. **34**, 155 (1996).
[2] P. Blasi, S. Burles, and A.V. Olinto, Astrophys. J. **514**, L79 (1999).
[3] R. M. Kulsrud, R. Cen, J. P. Ostriker, and D. Ryu, Astrophys. J. **480**, 481 (1997).
[4] M. J. Rees, Quart. J. Roy. Astron. Soc. **28**, 197 (1987).
[5] S. Furlanetto and A. Loeb, Astrophys. J. **556**, 619 (2001).

[6] D. Grasso and H. R. Rubinstein, Phys. Rep. **348**, 163 (2001).
[7] M. Giovannini, Int. J. Mod. Phys. D **13**, 391 (2004).
[8] M. Lemoine, G. Sigl, A.V. Olinto, and D. N. Schramm, Astrophys. J. **486**, L115 (1997).
[9] G. Sigl and M. Lemoine, Astropart. Phys. **9**, 65 (1998); G. Bertone, C. Isola, M. Lemoine, and G. Sigl, Phys. Rev. D **66**, 103003 (2002).
[10] R. Plaga, Nature (London) **374**, 430 (1995); A. Wingler, R. Plaga, and F. Krennrich, in *Proceedings of the 26th International Cosmic Ray Conference (ICRC 99), Salt Lake City, Utah, 1999*, edited by B. L. Dingus, D. B. Kieda, and M. H. Salamon, AIP Conf. Proc. No. 516 (Springer-Verlag, New York, 1999).
[11] K. Dimopoulos and A. C. Davis, Phys. Lett. B **390**, 87 (1997).
[12] D. T. Son, Phys. Rev. D **59**, 063008 (1999).
[13] K. Jedamzik, V. Katalinić, and A.V. Olinto, Phys. Rev. D **57**, 3264 (1998).
[14] K. Subramanian and J. D. Barrow, Phys. Rev. D **58**, 083502 (1998).
[15] In particular, magnetic fields are simply assumed frozen-in after the epoch of $e^{\pm}$ annihilation.
[16] A. Brandenburg, K. Enqvist, and P. Olesen, Phys. Rev. D **54**, 1291 (1996).
[17] M. Christensson, M. Hindmarsh, and A. Brandenburg, Phys. Rev. E **64**, 056405 (2001).
[18] J. M. Cornwall, Phys. Rev. D **56**, 6146 (1997).
[19] P. Olesen, Phys. Lett. B **398**, 321 (1997).
[20] G. B. Field and S. M. Carroll, Phys. Rev. D **62**, 103008 (2000).
[21] T. Vachaspati, Phys. Rev. Lett. **87**, 251302 (2001).
[22] G. Sigl, Phys. Rev. D **66**, 123002 (2002).
[23] K. Subramanian and J. D. Barrow, Phys. Rev. Lett. **81**, 3575 (1998).
[24] K. Subramanian and J. D. Barrow, Mon. Not. R. Astron. Soc. **335**, L57 (2002).
[25] A. Mack, T. Kahniashvili, and A. Kosowsky Phys. Rev. D **65**, 123004 (2002).
[26] K. Jedamzik, V. Katalinic, and A.V. Olinto Phys. Rev. Lett. **85**, 700 (2000).
[27] J. Stone and M. Norman, Astrophys. J. Suppl. Ser. **80**, 753 (1992).
[28] J. Stone and M. Norman, Astrophys. J. Suppl. Ser. **80**, 791 (1992).
[29] D. A. Clarke, R. A. Fiedler, and M. L. Norman, ZEUS3D User Manual (NCSA Technical Report No. 015, 1994), http://zeus.ncsa.uiuc.edu/lca_intro_zeus3d.html
[30] P. S. Iroshnikov, Sov. Astron. **7**, 566 (1964).
[31] R. H. Kraichnan, Phys. Fluids **8**, 1385 (1965).
[32] P. Goldreich and S. Sridhar, Astrophys. J. **438**, 763 (1995); J. Cho, A. Lazarian, and E. Vishniac, Lect. Notes Phys. **614**, 56 (2003).
[33] J. Maron and P. Goldreich, Astrophys. J. **554**, 1175 (2001).
[34] W.-C. Müller and D. Biskamp, Phys. Rev. Lett. **84**, 475 (2000).
[35] D. Biskamp, *Nonlinear Magnetohydrodynamics* (Cambridge University Press, Cambridge, UK, 1993).
[36] C. J. Hogan, Phys. Rev. Lett. **51**, 1488 (1983).
[37] P. G. Saffman, Phys. Fluids **10**, 1349 (1967).
[38] M. Lesieur, *Turbulence in Fluids* (Kluwer, Dordrecht, 1997).
[39] M. M. Mac Low, R. S. Klessen, A. Burkert, and M. D. Smith, Phys. Rev. Lett. **80**, 2754 (1998).
[40] D. Biskamp and W.-C. Müller, Phys. Rev. Lett. **83**, 2195 (1999).
[41] E. G. Blackman, Mon. Not. R. Astron. Soc. **344**, 707 (2003).
[42] A. Lazarian, E. T. Vishniac, and J. Cho, Astrophys. J. **603**, 180 (2004).
[43] F. H. Shu, Astrophys. J. **273**, 202 (1983).
[44] K. Subramanian, astro-ph/9708216.
[45] E. G. Zweibel, Astrophys. J. **567**, 962 (2002).
[46] This is with the exception that for particularly chosen initial conditions, i.e., $\mathbf{v}_i \neq \mathbf{v}_n$ exponential damping of fluid flows on the integral scale may occur.
[47] This annihilation period reduces the number of $e^{\pm}$ by a large factor $\sim 10^{10}$ and is completed at $T \approx 20$ keV, where the number of positrons has fallen below the number of electrons.
[48] It may be instructive to point out, that, irrespective of initial magnetic spectra, magnetic field strength and coherence lengths are correlated, through Eq. (39). One may thus formulate statements in either of these quantities, with the other given by Eq. (39).
[49] This assumes that the gas is sufficiently hot after reionization such that ion viscosity is negligible.
[50] Note that this growth of the integral scale is associated with dissipation of magnetic fields into heat and therefore amounts into a small increase of the baryon temperature.
[51] We do not consider evolutionary effects due to cosmic structure formation in this paper.
[52] Note that Eq. (80) displays a weak spectral index dependence, i.e., $1/\sqrt{n}$ on the RHS, and we have assumed $n = 3$ in Eqs. (80) and (81).
[53] K. Dolag, M. Bartelmann, and H. Lesch, Astron. Astrophys. **348**, 351 (1999); **387**, 383 (2002).
[54] R. Banerjee and K. Jedamzik, Phys. Rev. Lett. **91**, 251301 (2003).
[55] J. D. Jackson, *Classical Electrodynamics* (John Wiley & Sons, New York, 1975).
[56] S. Weinberg, *Gravitation and Cosmology* (John Wiley & Sons, New York, 1972).
[57] K. Enqvist, Int. J. Mod. Phys. D **7**, 331 (1998).
[58] A. Kercek, K. Jedamzik, T. Abel, and M.-M. Mac Low (unpublished).
[59] K. Jedamzik and G. M. Fuller, Astrophys. J. **423**, 33 (1994).
[60] P. J. E. Peebles, Astrophys. J. **142**, 1317 (1965).
[61] J. Ahonen and K. Enqvist, Phys. Lett. B **382**, 40 (1996).
[62] B. T. Draine, W. G. Roberge, and A. Dalgarno, Astrophys. J. **264**, 485 (1983).
[63] Elastic atomic scattering cross sections usually increase slightly with decreasing temperature.
[64] F. H. Shu, *The Physical Universe: An Introduction to Astronomy* (University Science Books, Mill Valley, CA, 1982).
[65] Information and the code to download are available from the Laboratory for Computational Astrophysics (LCA) at http://zeus.ncsa.uiuc.edu/lca_intro_zeus3d.html